Carbonate "clumped" isotope signatures in aragonitic scleractinian and calcitic gorgonian deep-sea corals

J. Kimball[1,2], R. Eagle[1,3], R. Dunbar[2],

[1] {Department of Atmospheric and Oceanic Sciences, Institute of the Environment and Sustainability, University of California, Los Angeles, CA, 90095, USA}

[2]{Department of Environmental Earth System Science, Stanford University, Stanford, CA 94025, USA}

[3]{European Institute of Marine Sciences (IUEM), Université de Brest, UMR 6538/6539, Rue Dumont D'Urville, and IFREMER, Plouzané, France}

Corresponding author: robeagle@g.ucla.edu

Abstract

Deep-sea corals are a potentially valuable archive of the temperature and ocean chemistry of intermediate and deep waters. Living in near constant temperature, salinity and pH, and having amongst the slowest calcification rates observed in carbonate-precipitating biological organisms, deep-sea corals can provide valuable constraints on processes driving mineral equilibrium and disequilibrium isotope signatures. Here we report new data to further develop "clumped" isotopes as a paleothermometer in deep-sea corals as well as to investigate mineral-specific, taxon-specific, and growth-rate related effects. Carbonate clumped isotope thermometry is based on measurements of the abundance of the doubly-substituted isotopologue $^{13}C^{18}O^{16}O_2$ in carbonate minerals, analyzed in CO_2 gas liberated on phosphoric acid digestion of carbonates and reported as Δ_{47} values. We analyzed Δ_{47} in live-collected aragonitic scleractinian (*Enallopsammia* sp.) and calcitic gorgonian (Isididae and Coralliidae) deep-sea corals, and compared results to published data for other aragonitic scleractinian taxa. Measured Δ_{47} values were compared to *in situ* temperatures and the relationship between Δ_{47} and temperature was determined for each group to investigate taxon-specific effects. We find that aragonitic scleractinian deep-sea corals exhibit higher values than calcitic gorgonian corals and the two groups of coral produce statistically different relationship between Δ_{47} -

temperature calibrations. These data are significant in the interpretation of all carbonate "clumped" isotope calibration data as they show that distinct Δ_{47}-temperature calibrations can be observed in different materials recovered from the same environment and analyzed using the same instrumentation, phosphoric acid composition, digestion temperature and technique, CO_2 gas purification apparatus, and data handling.

There are three possible explanations for the origin of these different calibrations. The offset between the corals of different mineralogy is in same direction as published theoretical predictions for the offset between calcite and aragonite although the magnitude of the offset is different. One possibility is that the deep-sea coral results reflect that crystals may attain nominal mineral equilibrium clumped isotope signatures only under conditions of extremely slow growth. In that case, a possible explanation for the attainment of disequilibrium bulk isotope signatures and equilibrium clumped isotope signatures by deep-sea corals is that extraordinarily slow growth rates can promote the occurrence of isotopic reordering in the interfacial region of growing crystals. We also cannot rule out a component of a biological "vital-effect" influencing clumped isotope signatures in one or both orders of coral. Based on published experimental data and theoretical calculations, these biological "vital" effects could arise from kinetic isotope effects due to the source of carbon used for calcification, temperature- and pH-dependent rates of CO_2 hydration and/or hydroxylation, calcifying fluid pH, the activity of carbonic anhydrase, the residence time of dissolved inorganic carbon in the calcifying fluid, and calcification rate. A third possible explanation is the occurrence of variable acid digestion fractionation factors. Although a recent study has suggested that dolomite, calcite, and aragonite may have similar clumped isotope acid digestion fractionation factors, the influence of acid digestion kinetics on Δ_{47} is a subject that warrants further investigation.

Introduction

"Clumped"-isotope paleothermometry is an approach to determining carbonate mineral formation temperatures (Ghosh et al., 2006; Schauble et al., 2006; Eiler, 2007), which like the oxygen isotope thermometer before it, is founded on thermodynamic predictions of the distribution of isotopes. Crucially, instead of relying on an isotopic exchange reaction between different phases (e.g. $CaCO_3$ and H_2O), clumped isotope thermometry relies on internal isotopic exchange between isotopes in a single phase (Schauble et al., 2006). This means that, in theory, all that is needed to determine mineral formation temperatures is the clumped isotope composition of the solid, and not the water from which it grew (Schauble et al., 2006; Eiler, 2007). When considering carbonate minerals, statistical thermodynamics predicts that heavy stable isotopes of carbon (^{13}C) and oxygen (^{18}O) will increasingly bond or "clump" in a mineral as temperature decreases and will conform to isotopic equilibrium constants for reactions such as:

[1] $X^{12}C^{18}O^{16}O_2 + X^{13}C^{16}O_3 <-> X^{12}C^{16}O_3 + X\mathbf{^{13}C^{18}O}^{16}O_2$

where X refers to cations such as Ca^{2+}, Mg^{2+}, Sr^{2+}, Ba^{2+}. In practice, the determination of ^{13}C-^{18}O bonds in carbonate minerals is accomplished by measurement of mass-47 CO_2 (predominantly $^{13}C^{18}O^{16}O$) liberated by phosphoric acid digestion Ghosh et al., 2006). ^{13}C-^{18}O bonding is reported as a per mil enrichment from that which would be expected in the liberated CO_2 if the sample had a stochastic distribution of C and O isotopes among all isotopologues and is designated by the parameter Δ_{47}. Following the initial calibration of synthetic calcites and some coral taxa (Ghosh et al., 2006), several studies have focused on in-depth calibrations of biogenic carbonates that represent potential paleoclimate proxies. Proxy material calibrations thus far have included aragonitic scleractinian zooxanthellate corals (Ghosh et al., 2006; Saenger et al., 2012; Tripati et al., 2015), aragonitic scleractinian non-zooxanthellate deep-sea corals (Ghosh et al., 2006; Thiagarajan et al., 2011), aragonitic otoliths (Ghosh et al., 2007), calcitic and aragonitic foraminifera (Tripati et al., 2010), mollusks and brachiopods (Came et al., 2007, 2014; Eagle et al., 2013; Henkes et al., 2013) and land snails (Zaarur et al., 2011; Eagle et al., 2013), calcitic speleothems (Affek et al.,

2008; Daëron et al., 2011), bioapatite (Eagle et al., 2010), and calcitic microbialites (Petryshyn et al., 2015).

It has been noted that calibration data on different biogenic carbonates generated in the same laboratory at Caltech and using similar analytical methods produce a relationship between temperature and Δ_{47} values that was similar to the initial inorganic calcite calibration (Ghosh et al., 2006; Eagle et al., 2013). However there are differences in inorganic calcite calibrations produced in different laboratories (Ghosh et al., 2006; Dennis and Schrag et al., 2010; Zaarur et al., 2013; Tang et al., 2014; Wacker et al., 2013; Kluge et al., 2015), that are thought to either reflect methodological differences in clumped isotope measurements or differences in how synthetic carbonates were precipitated (Tripati et al., 2015). It is clear from studies in mollusks (Henkes et al., 2013; Eagle et al., 2013; Douglas et al., 2014; Petrizzo et al., 2014) and brachiopods (Henkes et al., 2013; Came et al., 2014) that calibrations of the same types of materials in different laboratories can yield different relationship between temperature and Δ_{47} values.

More recent studies have discussed some possible sources of methodological effects on clumped isotope calibrations relating to data handling and mass spectrometric effects (Wacker et al., 2013; Petrizzo et al., 2014; Defliese et al., 2015). It is also possible that phosphoric acid digestion technique and temperature may be playing a role (Wacker et al., 2013; Defliese et al., 2015), as is known to be the case for conventional $\delta^{18}O$ measurements (Swart et al., 1991). Nonetheless carbonate standards and a deep-sea scleractinian coral were found to yield broadly comparable results in an inter-lab comparison study between four different laboratories (Dennis et al., 2011).

To date, there is relatively little published data attempting to resolve these whether different biogenic calibrations may originate from methodological differences between laboratories, by simply measuring multiple types of biogenic carbonates interspersed with each other using the same methods. Therefore it remains difficult at this time to distinguish between methodological differences and genuine differences in clumped isotope compositions of different materials, for example biologically mediated fractionations or "vital-effects". The little work that has been done includes *Porites* corals that appears to exhibit a kinetic isotope effect that drives their Δ_{47} values significantly out of equilibrium (Ghosh et al., 2006; Saenger et al., 2012), and a temperate coral *Oculina arbuscula* cultured at the same temperature and variable pH that exhibits large kinetic effects (Tripati et al., 2015).

Here we explore ^{13}C-^{18}O bond abundances in deep-sea coral species from the orders Scleractinia and Gorgonacea, that precipitate aragonite and high-Mg calcite respectively. As these corals were recovered from the same environment, analyzed by the same methods and mass spectrometer during the same analytical period, and subject to the same data processing, they represent an opportunity to explore the potential role of mineralogy and biology in governing clumped isotope signatures. We discuss results in the context of recent studies including of acid digestion fractionation (Defliese et al., 2015) and theoretical models and experimental data that have been used to constrain differences in clumped isotope composition between different dissolved inorganic carbon (DIC) species (Hill et al., 2014; Tripati et al., 2015), as it has been suggested that in cases where a carbonate mineral may inherit an isotopic signature of DIC then factors effecting DIC speciation such as pH, salinity, and temperature may also influence carbonate clumped isotope signatures (Hill et al., 2014; Tripati et al., 2015).

1.1 Deep-sea corals in paleoceanography

Deep-sea corals represent a potentially valuable archive of intermediate and deep ocean temperatures, and have been a target for models of stable isotope fractionation (Adkins et al., 2003; Gaetani et al., 2011). These archives could give valuable insight into the natural variability of regions of the ocean that play an active role in large-scale climate dynamics. With fossil deep-sea coral recorded for at least the last 225,000 years (Robinson et al., 2007; Thiagarajan et al., 2013) it is a proxy with potential to extend our observations of ocean physics and climate into the Pleistocene with decadal to centennial resolution. It has been established that deep-sea corals have significant skeletal "vital" effects (disequilibrium stable isotope fractionations) that compromise the classic $\delta^{18}O$ paleotemperature method (Emiliani et al., 1978; McConnaughey, 1989a, 2003; Adkins et al., 2003; Smith et al., 2000; Rollion-Bard et al, 2003, 2010; Lutringer et al., 2005; Hill et al., 2011, Kimball et al., 2014). Attempts to circumvent these kinetic effects have focused on the "lines" method that recovers an average temperature over the lifetime of a coral (Smith et al., 2000; Lutringer et al., 2005; Hill et al., 2011; Kimball et al., 2014) and a Rayleigh-based multi-element (e.g. Mg/Ca, Sr/Ca, Ba/Ca) paleotemperature method (Gaetani et al., 2011).

Despite deep-sea coral species showing significant disequilibrium in $\delta^{13}C$ and $\delta^{18}O$ values, sometimes termed "vital effects", initial calibration work using clumped-isotopes in scleractinian corals (Thiagarajan et al., 2011) revealed a good agreement between aragonitic scleractinian deep-sea coral Δ_{47} and the inorganic calcite calibration of Ghosh et al. (2006). Therefore at least some species that show significant "vital effects" on $\delta^{13}C$ and $\delta^{18}O$ yield apparent equilibrium Δ_{47} values, an observation also made on foraminifera and coccoliths (Tripati et al., 2010). Recently scleractinian deep-sea coral Δ_{47} measurements have been used in applied paleoceanographic reconstructions (Thiagarajan et al., 2014).

2 Samples and Methods

2.1 Samples

Thirteen live-collected specimens of deep-sea coral were examined. One specimen, PV 703-7 was mostly dead with patches of living tissue. Specimens were collected by deep-sea submersible diving on Warwick Seamount, Gulf of Alaska (DSRV Alvin, 2002), the Hawaiian Islands (DSRV Pisces V, 2007) and Line Islands (DSRV Pisces IV, 2005) (**Fig. 1**). The thirteen corals belong to the Gorgonacea (gorgonian) and Scleractinia (scleractinian) orders. Gorgonian corals represent the Isididae and Coralliidae families and scleractinian corals are *Enallopsammia rostrata*. Isididae samples were identified as *Keratoisis*, *Isidella*, or *Acanella* spp. (collectively referred to as bamboo corals) and the Coralliidae sample as *Corallium* sp., most likely *Corallium secundum* (**Table 1**). Identification at the time of collection represents the current and best available taxonomic understanding.

Temperature data from Warwick Seamount is averaged from two Seabird CTD casts taken at the dive location during the dive, while *in situ* temperature was measured on DSRV Pisces V and IV at the time of collection for Hawaiian and Line Island corals. Temperature ranges from Hawaiian Island coral were calculated from Hawaiian Ocean Time Series (HOTS) (data collected at Station ALOHA during the years 1990-2012. Although Station ALOHA is located about 328 miles east of our samples, a comparison between the HOTS vertical temperature profile matches closely to CTD profiles taken from the sample locations. Additionally, Station ALOHA was originally chosen as a monitoring station because it is believed to be representative of the North Pacific subtropical gyre and we take it to represent conditions experienced by Hawaiian corals. Temperature ranges from Warwick Seamount are

estimated from CTD casts taken at approximately 48.02N, -130.66W from 11 cruises during 1972-1998 at different times of the year. Temperature data was extracted from National Oceanic Data Center at 634± 5 m, 704± 5 m, 720±5 m and 872±5 m to assess temperature variability at the depths the corals were collected at, in the same oceanic region. Similarly temperature ranges from the Line Islands are estimated from CTD casts extracted from National Oceanic Data Center taken at approximately 6°N, -160°W from 9-27 cruises (depending on depth) during 1972-1998.

2.2 Sample preparation

Disks were cut from near the base for all coral skeletons, except PV 703-7 which was dead at the base. For this specimen, a disk was cut from the living branch for sampling. Disks were cleaned by the simple method of sonication in nanopure water and air-drying at room temperature (~ 25°C). All specimens lacked visual organic contamination of any kind and following the findings of Thiagarjan et al. (2011) and Eagle et al. (2013), which found cleaning steps to be unnecessary in deep-sea corals and mollusks, respectively, no further cleaning was performed. For most corals, sample powders of ca. 50-70 mg were milled using a Merchantek micromill from the outer portions of disks which represents the most recently accreted part of the skeleton (**Fig. 2**). In one sample, PV-703-5, a sample was milled from both the center and outer edge of the disk. In a few cases (PIV 148-2, PV 703-2 PIV 146-6, PV 694-3, PV 694-13) samples were first milled from the outer edge and later, to obtain additional sample, whole disks were ground into powder using a mortar and pestle. Although milling was preferred, in some cases, disks were small enough that the entire disk was necessary to yield the required weight of sample for replica Δ_{47} measurements.

In order to explore intra-coral heterogeneity and sampling effects, specimen PIV 146-6 is sampled both along the outer edge by micromilling as well as by grinding and homogenizing an entire disk, while PV 703-5 was micromilled in the center and outer edge (**Fig. 2**). In this way, intra-specimen reproducibility and the effects of sampling were assessed.

2.3 Notation and reference frame

The parameter Δ_{47} is a measure of the enrichment in per mil of $^{13}C^{18}O^{16}O$ in CO_2 relative to the predicted stochastic abundance:

$$\Delta_{47} = (R_{47}/ R_{47}^* -1) - (R_{46}/ R_{46}^* -1) - (R_{45}/ R_{45}^* -1) \times 1000$$

where R_{47}, R_{46}, R_{45} are the measured abundance ratios of masses 47/44, 46/44 and 45/44 in the sample and R_{47}*, R_{46}*, R_{45}* are the predicted abundance ratios of the same masses in the sample if it had a stochastic distribution of C and O isotopes among CO_2 isotopologues.

Standard gases of different bulk compositions were equilibrated at different temperatures (25 or 1000°C) and measured each day. Values of Δ_{47} are reported in the absolute reference frame (ARF) and calculated as described in another publication using equilibrated gases(Dennis et al., 2011). Published data are presented in the absolute reference frame with conversion of data from Thiagarajan et al., (2011) and Ghosh et al. (2006) to the ARF, as reported in Eagle et al. (2013).

2.4 Analytical measurement of Δ_{47}

Isotopic measurements were conducted on a dual inlet Thermo Scientific MAT 253 mass spectrometer coupled to a custom-built semi-automated sample digestion and purification system located at the University of California, Los Angeles. The set-up is modeled on that used at Caltech and Johns Hopkins, which are described in Passey et al. (2010) and Henkes et al. (2013). Samples were run during two separate time periods (winter: January 2013-March 2013, summer: May 2013-July 2013) and samples of scleractinian (aragonite) and gorgonian (high-Mg calcite) were run interchangeably during both time periods. For each analysis (previously referred to as extraction) 8-10 mg of material was used to yield sufficient gas to maintain a steady signal at extended counting times. Also, recent results suggest that digestion of samples that are significantly smaller might undergo secondary equilibration with water, resulting in elevated Δ_{47} values compared to >7 mg size samples (Wacker et al., 2013).

Mass spectrometric configuration was set to measure ion beams corresponding to m/z= 44, 45, 46 (amplified by 3×10^8 to 1×10^{11} Ω resistors) and 47, 48, 49 (amplified by 10^{12} Ω resistors) with the ion bean m/z=44 fixed at ~16V. Each analysis contains 8 measurements of 7 cycles between sample and reference gas with 26 seconds of integration per cycle. The total integration time of 1456 seconds is sufficiently long that errors should be able to approach shot noise error predictions (Thiagarajan et al., 2011; Huntington et al., 2009). Internal precision of Δ_{47} was ca. 0.005-0.012‰, 1σ (based on 8 measurements of 7 cycles of sample and reference gas comparison within a single analysis, (**Table 2, Suppl. 1**) and external precision was ca. 0.004-0.008‰, 1σ (determined from repeat analyses of standards, **Table 3**)

To increase external precision, samples were measured 3-7 times each, which resulted in standard errors for Δ_{47} of 0.002-0.010‰ for the corals in this study (**Table 2**).

The semi-automated sample digestion system allows for sample to be introduced as either a carbonate powder or a gas. Carbonate powders are introduced via a Costech autosampler which drops samples *in vacuo* into a common ~103% phosphoric acid ($\rho \approx 1.91$ mg/ml) bath held at 90°C and allowed to react for 20 minutes. Evolved CO_2 from acid digestion is then passed through a cooled ethanol trap (-78°C) and collected in a liquid nitrogen trap (-200°C). CO_2 is liberated by warming with the same ethanol trap (-78°C), and with a helium carrier gas, passes through a Porapak Q 120/80 mesh GC (gas chromatograph) column at -20°C and silver wool which removes organic contaminants and scavenges sulfur compounds, respectively. After GC passage, CO_2 is again collected in liquid nitrogen and undergoes one final cryogenic purification step *in vacuo* before introduction to the mass spectrometer. Gaseous CO_2 can also be prepared on a vacuum line and introduced using quartz tubes. A tube cracker which leads into the second cooled ethanol trap prior to the GC step allows CO_2 to pass through the autoline in the same way as carbonate samples, minus the common acid bath.

In addition to carbonate powders, on most days, at least one gaseous "equilibrated CO_2" sample is analyzed for use in defining the absolute reference frame for Δ_{47} measurements. Producing equilibrated CO_2 gases with varying bulk isotopic ($\delta^{13}C$ and $\delta^{18}O$) composition is accomplished by utilizing a very depleted CO_2 ($\delta^{13}C$= -25‰, $\delta^{18}O$= 3.6‰ VSMOW) and equilibrating Oztech CO_2 ($\delta^{13}C$= -3.6‰ VPDB, $\delta^{18}O$= 23.6‰ VSMOW) with isotopically "heavy" water (^{18}O enriched and produced by boiling house DI). These two isotopically end member gases are then either heated at 1000°C for 2 hours to produce a nearly stochastic distribution of isotopes among isotopologues, or equilibrated in a water bath held at 25°C. Equilibrated CO_2 is then cryogenically purified on a vacuum line and captured into quartz tubes. This procedure produces four isotopically unique gaseous CO_2 samples which define the empirical transfer function (ETF) used to covert Δ_{47} values to the ARF scale (Dennis et al., 2011). The carbonate standards Carrara Marble, Carmel Chalk, TV01, and 102-GC-AZ01 were run in concert with samples and were shown to have values that were indistinguishable from those determined in the Caltech lab (**Table 3**).

An acid fractionation factor of 0.092‰ was applied to all data and to theoretical predictions to normalize to previously reported data at 25°C (Henkes et al., 2013). In tables and figures, we

also report results calculated using a value of 0.082‰ (Passey et al., 2010; Defliese et al, 2015b) as well as other acid digestion fractionation factors (e.g., Wacker et al., 2013).

3 Results

3.1 Scleractinian coral Δ_{47}

When compared with previously reported deep-sea coral data the aragonitic scleractinian coral results from this study agree very closely to those measured in Thiagarajan et al. (2011) and Ghosh et al. (2006) (**Figs. 3** and **4**). Measured and predicted coral isotopic measurements are presented in **Table 4.**. Since specimen PV 703-7 was mostly a dead coral except in small sections when collected and therefore could have had a more complicated life history, it was excluded from calibration analysis. For the purpose of calibration, we focus on data from live-collected specimens to compare with *in situ* temperature measurements to eliminate any uncertainty in growth temperatures or post-formation dissolution when considering proxy systematics. When the scleractinian corals are combined with the data from Thiagarajan et al. (2011), a similar Δ_{47} –T relationship to that originally reported is found. In a plot of Δ_{47} vs. $10^6/T^2$ the linear regression of the 11 corals from Thiagarajan et al., (2011) (slope: 0.0643±0.008, intercept: -0.029±0.103, R^2=0.934) is almost identical to that of the combined data set of 14 scleractinian corals (slope: 0.0582±0.008, intercept: 0.0452±0.103, R^2=0.81). As noted in Thiagarajan et al., (2011) this is closely similar to that of the Ghosh et al. (2006) calibration of inorganic calcite (slope: 0.0620; intercept: -0.0021).

The temperature sensitivity of the combined scleractinian coral calibration (slope: 0.0582±0.008, intercept: 0.0452±0.103, R^2=0.81) was examined. At high (17.4°C) and low (2.3°C) temperatures, 95% confidence intervals of Δ_{47} give ±0.0165‰ and ±0.0105‰, which correspond to temperature uncertainties of ca. ±4-5°C and ±3-4°C, respectively. At the average temperature of the data set (9.6°C) uncertainty can be as good as ±0.0075‰ or ±2°C. Uncertainty in Δ_{47} is converted to uncertainty in temperature in accordance with Huntington et al. (2009).

3.2 Gorgonian coral Δ_{47}

Gorgonian deep-sea corals precipitate skeletal carbonate in the form of high-Mg calcite, with 5-10 mol % $MgCO_3$ (Noé and Dullo, 2006; Kimball et al., 2014). Compared to scleractinian deep-sea coral and all other previously reported biogenic carbonates, Δ_{47} is depleted in gorgonian deep-sea corals. In a plot of Δ_{47} vs. $10^6/T^2$, the linear regression through data derived from 9 gorgonian deep-sea corals analyzed in this study gives a significantly shallower slope (slope: 0.025±0.01, intercept: 0.403±0.129, R^2=.48) and Δ_{47} offset of ca. 0.04-0.07‰ in the temperature range of 3.2-11.2°C compared to scleractinian corals as well as compared to the Ghosh et al. (2006) calibration. It is however more similar to the inorganic calibration of Dennis and Schrag (2010) (**Fig. 3**). Temperature sensitivity of the gorgonian coral calibration was not examined due to poorness of fit (R^2=0.48).

3.3 Intra-specimen sampling

Intraspecimen measurements from sampling different portions of the skeleton gives insight into the Δ_{47} heterogeneity present in an individual coral. Specimen PIV 146-6 was sampled both along the outer edge by micromilling as well as by grinding and homogenizing an entire disk, while PV 703-5 was micromilled in the center and outer edge. In both corals, aliquots produced from a given sampling method are significantly different in bulk isotopes. PIV 146-6 has differing bulk isotopic compositions between the two aliquots of more than 1‰ in $\delta^{13}C$ and 0.4‰ in $\delta^{18}O$. PV 703-5 has almost a 3‰ difference in $\delta^{13}C$ and 0.5‰ in $\delta^{18}O$ (**Table 5**). Δ_{47} of the aliquots are approximately 0.03 and 0.02 different from each other in PIV 146-6 and PV 703-5, respectively. For PIV 146-6, the average of all 7 measurements is 0.791±0.008 and for the two aliquots the averages are 0.779±0.007 and 0.803±0.01. For PV 703-5 the average of all 6 measurements is 0.744±0.007 and the averages for the two aliquots are 0.734±0.005 and 0.754±0.010.

4 Discussion

4.1 Trends in deep-sea coral data

The scleractinian corals analyzed in this study are solely *Enallopsammia* sp. In contrast, the deep-sea corals presented in Ghosh et al. (2006) and Thiagarajan et al. (2011) are scleractinian *Desmophyllum*, *Enallopsammia*, and *Caryophyllia* sp . All scleractinian species precipitate a skeleton composed of aragonite, although growth habits vary between species. *Desmophyllum* sp., also known as cup corals, grow in a rosette shape, whereas *Caryophyllia* and *Enallopsammia* sp. have a dendritic growth habit. The *E.rostrata* specimens measured in Thiagarajan et al. (2011) allow comparison between deep-sea corals of the same species measured in this study.

The scleractinian deep-sea coral data from this study have values that overlap with those reported by Thiagarajan et al. (2011). In contrast, the gorgonian corals show significantly lower Δ_{47} values compared to the scleractinian corals for the same temperature range. An analysis of covariance (ANCOVA) between the scleractinian and gorgonian coral data gives a P value <0.01 which indicates that the differences between the two groups are statistically significant. This 0.04-0.07 ‰ offset between scleractinian and gorgonian corals is observed in non-acid digestion corrected Δ_{47} values. Possible explanations for this offset are discussed below.

4.2 Comparison with other published Δ_{47} calibration data sets

Since its inception, numerous theoretical, inorganic and biogenic calibrations have been put forward to calibrate the Δ_{47}- T relationship in different carbonate materials. To date, at least seven synthetic calibrations have been published (Ghosh et al., 2006; Dennis and Schrag, 2010; Zaruur et al., 2013; Tang et al., 2014; Defliese et al., 2015; Kluge et al., 2015; Tripati et al., 2015). Numerous biogenic carbonate materials have been studied to assess their agreement with inorganic and theoretical studies (Ghosh et al., 2006; Thiagarajan et al., 2011; Saenger et al., 2012; Eagle et al., 2013; Henkes et al., 2013). The scleractinian corals in this study agree well with the inorganic calibrations of Ghosh et al. (2006) and Zaruur et al. (2014) and Tripati et al., 2015, while the gorgonian corals show agreement with the Dennis

and Schrag (2010), Tang et al. (2014), and Kluge et al., 2015 inorganic calibrations (e.g., **Fig. 4)**.

4.3 Comparison with theoretical predictions

Theoretical modeling of Δ_{63} for different carbonate minerals (Schauble et al., 2006; Hill et al., 2014; Tripati et al., 2015) have been combined with theoretical acid digestion fractionations to give predicted Δ_{47} values for a variety of carbonate minerals. These predictions generally agree with measured inorganic and biogenic studies however are more depleted in Δ_{47} for a given temperature. Further, offsets due to mineralogy, while predicted in these theoretical modeling studies, have not been resolved in measured samples. Compared to deep-sea coral Δ_{47}, theoretical predictions are more depleted for aragonite, however the calcite prediction agrees well with the calcitic gorgonians from this study (**Fig. 5**). The offset of 0.03 ‰ between aragonite and calcite is on the lower end of what we observe. A recent theoretical modeling effort (Hill et al., 2014) has produced similar predicted Δ_{47} values for aragonite and calcite although with more depleted (less agreement) between predicted and observed aragonite Δ_{47} and a smaller offset between aragonite and calcite.

4.4 Acid digestion fractionation factor uncertainties

It is possible that uncertainties in the acid digestion fractionation factor for carbonates digested at 25 and 90 °C may account for some of the above offsets. Three values have been proposed for the acid digestion fractionation factor (AFF) for reporting data at 90 °C and converting to 25 °C on the absolute reference frame. To explore the sensitivity of results to choice of acid digestion fractionation factor, **Fig. 6-9** show calculations using a range of acid digestion fractionation factors of isotope ratios, and apparent deviations of measured isotopic ratios from isotopic equilibrium. Passey et al. (2010) calculates and uses a value of 0.081‰, whereas Henkes et al. (2013) suggests a value of 0.092‰ ± 0.012‰, which is within error of the Passey et al. (2010) value. Defliese et al. (2015) proposes a value of 0.082‰ ± 0.014‰, which is within error of both values,. In a recent study Wacker et al. (2013) suggests there may be mineral-specific acid digestion fractionation factors (AFF), which is also predicted in the theoretical study by Guo et al. (2009). Application of the Wacker et al. $\Delta^*_{25\text{-}90}$ correction to the aragonite and calcite Δ_{47} data can explain 0.009‰ of the 0.03-0.07‰ offset observed in our aragonite and calcite data. Based on theoretical predictions for dolomite (Guo et al., 2009), a further offset might be expected due to Mg incorporation in calcite. Still,

experimental (Wacker et al., 2013; Defliese et al., 2015) and theoretical (Guo et al., 2009) studies suggest acid digestion differences due to mineralogy may not be large enough to explain the ca. 0.04-0.07‰ offset that we observe.

Deep-sea coral Δ_{47} were corrected using $\Delta_{25\text{-}90}$ AFF of 0.082‰ (Defliese et al., 2015) - identical to the value from Passey et al., 2010, 0.092‰ (Henkes et al., 2013) and 0.066‰ (Wacker et al., 2013, aragonite) and 0.075‰ (Wacker et al., 2013, calcite). **Figure 6** shows the result of the AFF sensitivity analysis and indicates that although the absolute values of the Δ_{47} change with application of AFF values, the offset between aragonite and calcite is unaffected except for in the case of application of mineral specific AFF from Wacker et al. (2013). Application of Wacker et al. (2013) mineral specific AFF values results in a decrease of the offset between the aragonite and calcite deep-sea coral Δ_{47} of only 0.009‰, therefore not altering our conclusions.

However, we acknowledge the kinetics of acid digestion and effects on clumped isotope signatures on Δ_{47} values is relatively poorly constrained. It is possible there are variable acid digestion fractionation factors that are influencing these observations, possibly due to cation substitution into carbonates (Guo et al., 2009), mineral bulk isotope composition (Guo et al., 2009), the presence of organic matter, as well as other factors. Until systematic studies of acid digestion is undertaken to investigate each of these factors, the contribution of acid digestion fractionation to the observed differences between aragonitic scleractinian and high-Mg calcitic gorgonian corals cannot be accurately quantified.

4.5 Analytical procedure, data comparison

Since its inception, the analytical measurement of Δ_{47} has improved in precision and accuracy due to advances in mass spectrometric analysis (e.g. development of automated sample digestions and purification systems, abbreviated to autoline, and higher counting times) and standardization of reporting procedures (Huntington et al., 2009; Dennis et al., 2011). Because the methods involved in producing and reporting Δ_{47} have changed over time, the comparison of data between laboratories and even within laboratories can be an issue. For relevant comparisons between previously reported data and this study's data, we refer to the recalculations of Δ_{47} performed in Eagle et al., (2013) using standard values to project into the absolute reference frame. Still, we can not exclude the possibility that analytical artifacts remain. For instance, Zaruur et al. (2013) noted that the shorter counting times and fewer

replications of the trailblazing work of Ghosh et al., (2006) may contribute to any discrepancies between data sets. We assess interlaboratory comparability from standards, which indicate accuracy and precision comparable to what has been reported for other laboratories (**Table 2**; Dennis et al., 2011). Furthermore, we note that good agreement between the aragonitic scleractinian corals of this study and that of Thiagarajan et al. (2011) reinforces the comparability of our data to the wider body of measurements reported from other laboratories.

Interlaboratory comparability should not be a critical issue for the interpretation of data presented herein since the offset between aragonitic and calcitic corals was observed in data generated within our lab, while running samples interchangeably using the same analytical procedure. Standards were also run concurrently during these time periods (**Table 3**) and found to be in good agreement with accepted values. We therefore conclude it is unlikely that the offset is due to internal analytical variability.

4.6 Mixing and intraspecimen Δ_{47} heterogeneity

It has been shown that both scleractinian and gorgonian deep-sea corals exhibit significant disequilibrium in $\delta^{13}C$ and $\delta^{18}O$ of several per mil within an individual coral (eg. Smith et al., 2000; Adkins et al., 2003; Rollion-Bard et al., 2003, 2010; Lutringer et al., 2005; Kimball et al., 2014). Because of the subtle saddle-shaped curvature in Δ_{47} relative to $\delta^{13}C$ and $\delta^{18}O$ (Eiler and Schauble, 2004; Thiagarajan et al., 2011; Defliese and Lohmann, 2015), Δ_{47} is sensitive to mixing of end member $\delta^{13}C$ and $\delta^{18}O$ values and will result in non-conservative mixing (**Fig. 10**). Deep-sea corals, with their several per mil range in $\delta^{13}C$ and $\delta^{18}O$ values will be particularly susceptible to this effect. In fact, both banding and spatial variability in $\delta^{13}C$ and $\delta^{18}O$ values within deep-sea coral skeletons varies on the scale of 10s to 100s of microns (Smith et al., 2000; Adkins et al., 2003; Rollion-Bard et al., 2003, 2010; Lutringer et al., 2005; Kimball et al., 2014). Any small-scale spatial variability makes the possibility of sampling within a skeletal band or an area with homogenous $\delta^{13}C$ and $\delta^{18}O$ values for Δ_{47} measurements unfeasible, and therefore there is the potential for mixing effects in Δ_{47} which we address here.

Both Thiagarajan et al. (2011) and Henkes et al. (2013) have addressed mixing in biogenic carbonates by calculating the Δ_{47} effect from mixing samples of differing bulk isotope composition. The end members from the Thiagarajan et al. (2011) calculations are similar to

the most extreme values that we observe ($\delta^{13}C$= 2‰, $\delta^{18}O$= 5‰ and $\delta^{13}C$= -10‰, $\delta^{18}O$= -2‰). Using these end member values, Thiagarajan et al. (2011) calculated a positive Δ_{47} increase as large as 0.02‰ for the resulting mixture, if 50% of each end member is used. They note that while this mixing effect is not consistent with their data, mixing and then re-equilibration could potentially result in the trend seen in their data. Since sampling an isotopically homogenous area of a deep-sea coral is unfeasible (especially given the sample size requirements for clumped isotopes), we estimate the maximum artifacts in our data arising from mixing. The estimate for mixing artifacts from Thiagarajan et al. (2011) is based on observed variability in stable isotope values in scleractinian deep-sea coral, and represents an extreme example for this study, as they use $\delta^{13}C$ and $\delta^{18}O$ values of end members that differ by 12‰ and 7‰, respectively. Such differences in scleractinian coral represent systematic isotopic depletions in centers of calcification compared to fibers (Adkins et al., 2003), as well as variability associated with density bands; no centers of calcification have been reported in gorgonian corals. The calculations from Thiagarajan et al. (2011) represent an estimate of the maximum artifact to arise from mixing for either taxa given the range of carbon and oxygen isotope values observed in scleractinian and gorgonian deep-sea coral. We also observed little variability in $\delta^{13}C$ and $\delta^{18}O$ of different preparations of the same coral, with standard deviations of <1‰.

As a further investigation into intraspecimen heterogeneity effects on Δ_{47} portions of two coral samples that differed in bulk isotopic composition were analyzed. In two corals, PIV 146-6 (scleractinian) and PV 703-5 (gorgonian), $\delta^{13}C$, $\delta^{18}O$ and Δ_{47} were measured from intraspecimen aliquots of carbonate produced from sampling portions of the skeleton which differed significantly in their bulk isotopic composition (**Table 5**). Although Δ_{47} of the aliquots are approximately 0.02‰ different from each other in both corals, this is similar to that reported in other studies between a few replicates (Huntington et al., 2009; Thiagarajan et al., 2011). Additionally there is not a consistent trend observed between $\delta^{18}O$ and Δ_{47}, as for coral PIV 146-6, the aliquot with the more positive $\delta^{18}O$ also has the higher Δ_{47}, but the opposite is observed for coral PV 703-5. We therefore interpret the difference in Δ_{47} values between the aliquots as noise in the measurements, which further reinforces the need to run many replicates.

4.7 Diffusion

Both Thiagarajan et al. (2011) and Saenger et al. (2013) have suggested the diffusion of CO_2 across the calicoblastic membrane in corals as a possible mechanism for fractionation of Δ_{47}. A generalized schematic of a scleractinian coral calcifying region is shown in **Fig. 11**. Thiagarajan et al. (2011) calculated 0.7‰ and 1.6‰ decreases in $\delta^{18}O$ and $\delta^{13}C$, respectively and a 0.036‰ increase in Δ_{47} for liquid phase diffusion of CO_2 (**Fig. 10**). For this Δ_{47} fractionation to be heritable by the mineral, however, the mineral must preserve the isotopic state of ordering of the DIC rather than obtain internal equilibrium within the mineral carbonate itself. Additionally carbonate mineral growth would have to occur before isotope clumping could reach equilibrium. Furthermore this fractionation only applies to DIC produced from diffused CO_2 and therefore the ratio of DIC from diffused DIC to 'DIC derived from seawater "leaking" directly to the calcifying environment would also have to be known. Both Thiagarajan et al. (2011) and Saenger et al. (2013) found fractionation associated with CO_2 diffusion across the calicoblastic layer or, additionally proposed by Saenger et al. (2013), across a boundary layer developed between the growing mineral and calcifying fluid, to be an unlikely explanation of the trends observed in their data. Additionally, gorgonian corals are not known to have calicoblastic cells (Noé and Dullo, 2006) so this is relevant to scleractinian corals, or if there is a similar functional cell playing a role in this for gorgonian corals.

It is possible the observed pattern could be explained if scleractinian deep-sea corals contain a larger fraction of diffused CO_2 compared to gorgonian coral, if this CO_2 then underwent relatively little isotopic equilibration in the calcifying fluid (**Fig. 10**). In cross plots of $\delta^{18}O$ and Δ_{47} residuals, scleractinian corals do exhibit elevated Δ_{47} and depleted $\delta^{18}O$ values, relative to Zaruur et al. (2013), Dennis and Schrag (2010) and theoretical aragonite (Schuable et al., 2006; Guo et al., 2009) in accordance with calculated diffusion effects. However, since scleractinian deep-sea corals generally conform to the majority of reported biogenic and synthetic calibrations, this would have be a widespread effect occurring in other materials reported as well.

4.8 Mineralogy and Δ_{47}

Despite Epstein et al.'s (1953) original finding that the nacreous layer (aragonite) and prismatic layer (calcite) of mollusks showed no oxygen isotopic offset, it has since been

recognized that aragonite is enriched in ^{18}O and ^{13}C relative to calcite both in theory and experiment (Tarutani et al., 1969; Kim and O'Neil, 1997; Kim and O'Neil, 2007; Mavtomatis, 2012). An analogous mineralogical offset is predicted for Δ_{47} (with aragonite predicted to have greater abundance of ^{13}C-^{18}O bonds than calcite that formed at the same temperature) (Schauble et al., 2006; Guo et al., 2013; Hill et al., 2014; Tripati et al., 2015).

The corals in this study differ in mineralogy, with scleractinian corals precipitating a fully aragonitic skeleton and gorgonian corals secreting carbonate in the form of high-Mg calcite. To date, a combination of aragonitic and calcitic biogenic materials have been analyzed. Calcitic specimens have been represented by certain species of mollusks (Eagle et al, 2013; Henkes et al., 2013), brachiopods (Came et al., 2007; Henkes et al., 2013), and foraminifera (Tripati et al., 2010). Aragonitic specimens have included deep-sea (Thiagarajan et al., 2011) and shallow (Ghosh et al., 2006; Saenger et al., 2013) scleractinian corals, mollusks (Eagle et al., 2013; Henkes et al., 2013), and land snails (Zaarur et al., 2011), all of which have not revealed statistically significant mineralogical offsets from the synthetic calibrations of calcite (Ghosh et al., 2006; Dennis et al., 2010; Zaruur et al., 2013). More careful study, however of the XRD data of Ghosh et al. (2006) has revealed aragonite was also present in their precipitates (Zaruur et al., 2013).

Despite not observing this offset between calcite and aragonite Δ_{47} in synthetic or biogenic carbonates, it has been predicted in theoretical studies. By combining a previous theoretical model of ^{13}C-^{18}O clumping in carbonate minerals (Schauble et al., 2006) with their theoretical model of kinetic isotope effects associated with phosphoric acid digestion, Guo et al. (2009) proposed predicted Δ_{47}- T relationships for a number of carbonate minerals. For the temperature range 0-30°C, $\Delta_{47,\ \text{aragonite-calcite}} \approx 0.02‰$ and $\Delta_{47,\ \text{aragonite-dolomite}} \approx 0.04‰$ with the direction of fractionation in agreement with the offset that we observe (**Figure 5**). A similar pattern was reported by Hill et al. (2014) and Tripati et al. (2015). If these models of mineral-specific Δ_{47}-T relationships is correct, then this could potentially explain a substantial portion of the offset we observe between the aragonite and high-Mg calcite corals in this study. We discuss possible reasons for observed mineralogical effects in deep-sea corals and not in other types of carbonates in more detail below.

4.8 Calcification in scleractinian deep-sea corals

Non-equilibrium partitioning of oxygen and carbon isotopes have been observed in numerous calcifying organisms and inorganic precipitation experiments, and linked to calcification processes (e.g. McConnaughey, 1989a; Spero et al., 1997; Zeebe, 1999; Adkins et al, 2003: Watson, 2004; DePaolo, 2011; Gabitov et al., 2012; Watkins et al., 2013). Clumped isotopes represent another tool that can be used to probe mechanisms for disequilibrium isotopic signals in biological carbonates, and to determine when equilibrium precipitation has occurred, through the coupling of theoretical calculations and inorganic precipitation experiments with culturing studies (Thiagarajan et al., 2011; Tripati et al., 2015). **Fig. 10** shows a framework for how multiple paired stable isotope measurements can be used to trace the origin of disequilibrium effects.

In scleractinian corals, precipitation of carbonate is believed to occur in a space between the calicoblastic layer and the hard skeleton (**Fig. 11**). It is likely that calcifying fluid chemistry (pH, salinity) as well as growth rate and DIC equilibrium can all be potential sources of non-equilibrium signals preserved in the solid. The chemical composition and DIC sources from which the carbonate mineral forms have been a main focus for understanding non-equilibrium $\delta^{13}C$ and $\delta^{18}O$ values observed in corals. Biomineralization in shallow symbiotic scleractinian corals has been well-studied over the past few decades (see Cohen and McConnaughey, 2003 for a review). Early studies of shallow symbiotic scleractinian corals revealed time independent $\delta^{18}O$ and $\delta^{13}C$ offsets from theoretical carbonate-water fractionation curves. This was addressed through species-specific calibration studies, which allowed offsets to be corrected for, revealing the underlying environmental signals (Weber and Woodhead, 1972; Dunbar and Wellington, 1981). In contrast, linear trends between $\delta^{18}O$ and $\delta^{13}C$ with depletions of several per mil, are observed in an individual deep-sea coral. Living in near constant temperature, salinity and pH environments, these large disequilibrium signals are attributed to their biomineralization mechanism (i.e. "vital effects"). Different mechanistic models aimed at explaining non-equilibrium $\delta^{13}C$ and $\delta^{18}O$ values seen in deep-sea corals have been proposed to account for these so-called "vital effects".

The first of these models, proposed by McConnaughey (1989a) calls on a kinetic fractionation during the hydration and hydroxylation steps of DIC speciation in which precipitation outpaces the ability of the system to reach isotopic equilibrium ("Kinetic model" in **Fig. 11**). The range of $\delta^{13}C$ and $\delta^{18}O$ values is therefore a reflection of a spectrum of varying amounts

of equilibrium being attained amongst DIC species. The master variable in this case being time, McConnaughey (1989b), using calcification rates, calculated that calcification could outpace the time it took for isotopic equilibrium to be reached. Henkes et al. (2013) further noted that at lower temperatures, days to weeks are required for oxygen isotopic equilibrium to be reached in DIC.

The second model proposed by Adkins et al. (2003) extensively examines potential sources of DIC to the extracellular calcifying fluid and introduces the concept of a variable pH environment as the master controller on skeletal $\delta^{13}C$ and $\delta^{18}O$ ("pH model" in **Fig. 11**). For oxygen isotope processes, they draw on work characterizing the oxygen isotopic fractionation between DIC species (i.e. CO_2, H_2CO_3,, HCO_3^-, CO_3^{2-}) (McCrea, 1950; Usdowski et al., 1991; Zeebe and Wolf-Gladrow, 2001; Beck et al., 2005; Zeebe, 2007; Rollion-Bard et al., 2011). Their model suggests that the mineral preserves the oxygen isotopic ratio of HCO_3^-/CO_3^{2-}. Because each DIC species has a unique oxygen fractionation relative to water, the oxygen isotope fractionation between the sum of DIC (DIC_{sum}) species and water will vary depending on the proportion of the DIC species. For seawater, at high pH (pH >9), DIC will be dominated by CO_3^{2-}, which has the lowest fractionation factor and will therefore result in a more depleted $\delta^{18}O$ value of the DIC_{sum} from which the mineral precipitates. At lower (pH 6-9) fluid pH, as the HCO_3^-/CO_3^{2-} ratio of the fluid rises, so does the precipitated mineral's $\delta^{18}O$ value. $\delta^{13}C$ is not expected to be sensitive to pH effects since the exchange of carbon between DIC species is very rapid. $\delta^{13}C$, therefore, is proposed to be a function of two sources of CO_2, membrane diffused and seawater leaked, and the proportion of them, a function of pH gradients across the membrane. The 'break' that they uncover at the most depleted isotopic values in which $\delta^{18}O$ continues to decrease but $\delta^{13}C$ plateaus, is interpreted as the point at which the maximum flux of diffused CO_2 across the membrane is reached (during rapid calcification). Qualitatively their model captures the isotopic trends that they see in their corals and although numerical modeling is able to reproduce the 'break' and range of $\delta^{18}O$ and $\delta^{13}C$ that they report, it fails to reproduce the numerical value of the $\delta^{18}O$ vs. $\delta^{13}C$ slopes that they observe. $\delta^{18}O$ vs. $\delta^{13}C$ slopes have been observed in other studies and appear to be a conservative property of biomineralization in deep-sea corals (Smith et al., 2000; Adkins et al., 2003; Rollion-Bard et al. 2003, 2010; Lutringer et al 2005; Hill et al., 2010; Kimball et al., 2014). Discrepancies between the biomineralization model of Adkins et al., 2003 and boron isotope data are yet to be resolved (Blamart et al., 2007; Rollion-Bard et al., 2010).

Additional biomineralization models have been proposed in shallow symbiotic corals which incorporate the presence and activity of zooxanthellae (Cohen and McConnaughey, 2003; Rollion-Bard et al., 2003; Allison et al., 2010) and for deep-sea corals (Rollion-Bard et al., 2010; Gaetani et al., 2010). However only those models that examine effects on $\delta^{18}O$ and $\delta^{13}C$ are considered with respect to the data presented herein.

More generally, models for equilibrium/disequilibrium stable isotope signatures have been proposed that examine processes that influence the ion-by-ion growth of crystals (Nielsen et al., 2012; Watkins et al., 2013; Tripati et al., 2015), as well as diffusional/reordering processes that occur near the calcifying fluid/crystal interface (Watson and Liang, 1995; Watson, 2004; Gabitov et al., 2012; Tripati et al., 2015).

4.9 Calcification in gorgonian deep-sea corals

The growth structure, mineralogy, and biomineralization of gorgonian coral skeletons is distinctly different from scleractinian corals (Noé and Dullo, 2006). Additionally, the organic matrix-mediated calcification process is largely unexplored and unknown for most gorgonian families. The biomineralization models described for scleractinian corals therefore are not valid when interpreting potential vital effect signals in gorgonian corals.

An exhaustive study of the growth structure and fabric of deep-sea isidid gorgonians in the same family as those investigated here, was done by Noé and Dullo (2006). Their findings are based on characterization of the isidid skeletal micro- and ultrastructure in combination with absolute age determinations. From their reconstructions of growth mode and fabric, they propose a biomineralization model. With no calicoblastic cells observed in gorgonians, they propose gorgonin produced from the endodermal epithelium acts as the structural framework, while a viscous slime surrounding the skeleton acts as the matrix, facilitating and regulating mineral growth. Their model however relies on physical observations and lacks geochemical data to inform their interpretations. So while offering some insight into the uniqueness of Isidid biomineralization, the findings are not useful in interpreting the geochemical data observed in this study.

Despite the lack of proposed biomineralization models in gorgonian corals, the trends in $\delta^{13}C$ and $\delta^{18}O$ have been explored and found to be similar in pattern to scleractinian corals, but with an offset that agrees with theoretical mineralogical fractionation predictions. The

similarity in $\delta^{13}C$, $\delta^{18}O$ and δ_{47} patterns suggests that while the particular biomineralization process is necessarily different in the two groups, there is a functional similarity that results in the conserved patterns in both gorgonian and scleractinian corals.

4.9 Δ_{47} in deep-sea coral skeletal carbonate: biomineralization model implications

The Δ_{47} of a mineral is predicted to conform to the K_{eq} of a homogenous isotope exchange reaction (**Reaction 1**) and be independent of the fluid composition from which is forms, as well as the bulk isotopic composition of the crystal. Recent experimental and theoretical studies have suggested that mineral equilibrium with respect to Δ_{47} might not always be attained however (Saenger et al., 2013; Tripati et al., 2015). Because of this, Δ_{47} can be utilized as an additional geochemical skeletal signal which could give more insight into the mechanisms involved in skeletal precipitation in deep-sea corals and other biological carbonates.

In a recent study, (Tripati et al., 2015) the impact of DIC speciation on mineral Δ_{47} signatures was examined with respect to Δ_{47}. Contrary to initial theoretical modeling by Hill et al. (2014) which calculated differences of ~0.03‰ in the Δ_{47} values of DIC species at equilibrium, Tripati et al. (2015), using experimental results, found that HCO_3^- Δ_{63} could be as much as 0.05 to 0.07‰ higher than CO_3^{2-}. They further propose that this fractionation could be partially or fully inheritable by the solid. Central to their mechanism of preservation of disequilibrium mineral Δ_{63} signals is the concept of differing mineral isotopic archival effects occurring during "slow" and "fast" crystal growth, with "slow" and "fast" being defined as particular to a specific temperature, salinity and pH growth environment, rather than conforming to a particular value. Depending on the proportion of HCO_3^- and CO_3^{2-} incorporated into the growing crystal and the ability of the crystal lattice to conform to K_{eq} (Reaction 1), disequilibrium in Δ_{63} and therefore Δ_{47} could be preserved. Only during "slow" crystal growth, they argue, is the mineral able to fully conform to K_{eq} (Reaction 1). In this scenario, disequilibrium in Δ_{63} and bulk isotopes are not correlated and it would therefore be possible to attain equilibrium with respect to Δ_{63}, but not in bulk isotopes (Tripati et al., 2015).

Deep-sea corals, being one of the slowest calcifiers, are a likely potential candidate for attainment of Δ_{63} mineral equilibrium, if the mechanism proposed by Tripati et al. (2015) is

correct. Bulk isotopes, as previously mentioned, vary greatly within an individual deep-sea coral, while Δ_{47} values are reproducible within instrumental error. This indicates that while bulk isotopes are controlled by processes such as in the biomineralization models outlined above, Δ_{47} values are independent and possibly conform to equilibrium values. While a complete quantitative biophysical model has yet to be proposed, one possibility is that the range in bulk isotopes is controlled by processes related to the chemical environment (eg. calcifying solution pH, kinetics) while the slow growth rates in deep-sea corals allow isotopic reordering at the crystal-solution interface resulting in attainment of nominal mineral equilibrium for Δ_{47} (**Fig. 11**).

Adkins et al. (2003), however, finds that in the more dense (interpreted as faster calcification) growth bands, $\delta^{18}O$ is depleted compared to the less dense (more slowly growing) bands. In the Tripati et al. (2015) model, they predict that during rapid calcification both $\delta^{18}O$ and Δ_{47} would be more positive. Relative to the calcification rates required for inheritance of these signals however, perhaps even at the most elevated calcification rates, deep-sea corals, are still able to reach mineral isotopic equilibrium with respect to Δ_{47}, while bulk $\delta^{18}O$ and $\delta^{13}C$ is still under the control of processes associated with the calcifying fluid environment.

Cross plots of $\delta^{18}O$ and Δ_{47} residuals (**Figs 7, 8, and 9**) can be used to assess conformation to proposed biomineralization models. For the McConnaughey et al. (2003) model of coral biomineralization, a range of depletions in $\delta^{18}O$ is expected, with coral $\delta^{18}O$ approaching or potentially reaching mineral equilibrium $\delta^{18}O$, depending on the calcification rate. Similarly in the Adkins et al. (2003) model, a range of pH would result in a range of depletions in recorded mineral $\delta^{18}O$, assuming that the proportion of HCO_3^-/CO_3^{2-} incorporated into the skeleton is independent of calcification rate (**Fig. 10**). Although neither model addresses Δ_{63}, in both cases, all else being equal, and assuming a mechanism for inheritance of DIC Δ_{63} into mineral Δ_{63}, a decrease in $\delta^{18}O$ would be tied to a decrease in Δ_{63}. For the McConnaughey et al. (2003) model, an increase in calcification rate resulting in only partial equilibration of the DIC-water system would result in depleted $\delta^{18}O$ and Δ_{63} values of HCO_3^- and CO_3^{2-}. Similarly, in Adkins et al. (2003) model, varying solution pH would have the same effect on $\delta^{18}O$ and Δ_{63} with both values decreasing (increasing) as pH increases (decreases). Comparing residual cross plots from various Δ_{47} calibrations however, fails to capture a positive relationship between $\delta^{18}O$ and Δ_{47} and instead appears that $\delta^{18}O$ and Δ_{47} are varying independently from each other. This suggests that either the models are not accurately

portraying the mechanism by which variable $\delta^{18}O$ values are inherited in the mineral or the Δ_{63} is not under the same controls as $\delta^{18}O$ (i.e. not inheriting the Δ_{63} value of the fluid).

4.10 Other biomineralization effects

Unlike scleractinian zooxanthellate and azooxanthelate corals, gorgonian corals have been much less studied. In particular, biomineralization in gorgonian corals has yet to be addressed from a geochemical perspective. The fact that gorgonians precipitate high-Mg calcite however, in contrast to the aragonitic skeletons of scleractinians, is a simple indication of differing biomineralization mechanisms (Ries, 2010). Additionally, although it has been shown that deep-sea gorgonian corals exhibit $\delta^{18}O$ and $\delta^{13}C$ trends similar to their scleractinian counterparts, they have not been shown to exhibit the 'break' that is observed in Adkins et al. 2003 (Kimball et al., 2014). When growing inorganic carbonate precipitates, mineralogy can be controlled through the Mg/Ca ratio of the precipitating fluid, with molar Mg/Ca>2 producing aragonite and high-Mg calcite and molar Mg/Ca<2 producing calcite (reviewed by Ries, 2010). Current seas are ca. Mg/Ca=5.2 (Ries, 2010) and the biomineralization mechanism responsible for precipitation of high-Mg calcite in gorgonians is unknown.

One possibility is that biomineralization is regulated in gorgonians through an organic template. The presence of an insoluble organic matrix in both isidid bamboo and *Corallium* sp. (Allemand et al., 1994; Ehrlich et al., 2006; Noé and Dullo, 2006) supports the possibility that an organic template may be directing mineral precipitation. The presence of an organic matrix is unique to gorgonian corals (has not been observed in scleractinians) and only preliminary studies have been undertaken to characterize the amino acid composition of the organic matrixes (Allemand et al., 1994; Ehrlick et al., 2006).

It seems plausible, that the organic template, in addition to directing lattice structure, could also be influencing isotopic fractionation within a growing mineral, as has recently been shown for Mg/Ca ratios in carbonates (Wang et al., 2009). Therefore, in addition to theoretical depletions expected in Δ_{63} due to mineralogy, the presence of an organic template might act as an additional control on bond ordering. Carbonate anhydrase has also been implicated in scleractinian hermatypic coral biomineralization models, and presence/absence and variable activities of carbonic anhydrase may another factor to be considered.

4.11 Suggestions for future work

In-depth experimental studies are needed to explore the role of multiple processes on acid digestion kinetics, such as Wacker et al. (2013) and Defliese et al. (2015). Possible factors influencing acid digestion fractionation factors that still need to be examined include (but are not limited to) organic matter content, the influence of cation substitution (e.g., high vs low Mg-calcite), variations in bulk composition ($\delta^{13}C$, $\delta^{18}O$), the type of reaction vessel and clean-up method used, and phosphoric acid composition.

Direct constraints on the impact of variable cation concentrations on the clumped isotopic composition of carbonate minerals from theory and synthetic experiments may be a useful tool to distinguish between whether these different deep-sea corals orders in fact are recording equilibrium mineral-specific offsets. Additionally, measurement of coral calcifying fluid pH and the use of labeled carbon sources during growth experiments would provide important constraints on whether the observed patterns reflect kinetic effects.

A unifying model which explains the observed patterns of isotopic and trace element variability that have been observed could also help to test the different explanations posed in this study and other publications, and could help us advance our understanding of biomineralization in scleractinian and gorgonian deep-sea corals. For clumped isotopes, such a model would need to include the factors that influence equilibrium fractionation, i.e., temperature and well-constrained mineral-specific fractionation factors. Additional factors that need to be included to accurately model kinetic isotope effects include temperature, the carbon source used for calcification (the relative fraction of seawater-derived DIC versus CO_2 diffused across cellular membranes), DIC speciation as controlled by multiple factors (pH, temperature, salinity), the timescale for DIC equilibration vs precipitation rate (affected by the residence time of DIC in the calcification space), as modulated by the occurrence and activity of the enzyme carbonic anhydrase.

5 Conclusions

Two groups of deep-sea corals with differing mineralogy (aragonite and calcite) were analyzed for $\delta^{13}C$, $\delta^{18}O$ and Δ_{47}. Aragonitic scleractinian deep-sea coral exhibit a nearly coincident Δ_{47}-T relationship to previously reported scleractinian deep-sea corals (Thiagarjan et al., 2011) and can be used to predict temperatures to ±2°C at the mean temperature and ±3-

5°C at the extreme ends of the data set. Calcitic gorgonian deep-sea corals show lower Δ_{47} values. This offset between taxa is consistent with theoretical predictions for mineralogic differences, albeit significantly larger in magnitude than expected. Therefore the offset between gorgonian and scleractinian deep-sea corals may reflect, at least in part, as a difference in mineralogy that is only observed in deep-sea corals and not in data published for other carbonates simply because of their very slow growth rates as compared to all other studied carbonates. Another equally likely explanation is that differences in carbon sources and biomineralization pathways in coral taxa result in distinctive clumped isotope vital effects in gorgonian and scleractinian deep-sea coral. Finally, we can not preclude that offsets may reflect variable acid digestion kinetics for the different types of materials that we have surveyed.

Data availability

All raw data for samples and standards and equilibrated gas lines are in Supplement 1.

Acknowledgements

This work was supported by a NSF Graduate Fellowship, NSF OCE-1437166, DOE BES grant DE-FG02-13ER16402, and the "Laboratoire d'Excellence" LabexMER (ANR-10-LABX-19), co-funded by a grant from the French government under the program "Investissements d'Avenir". We thank Aradhna Tripati and the Tripati Lab Group for their assistance with analyses and discussion of this work, and Ben Elliott for assistance with drafting figures.

References

Adkins, J.F., Boyle, E.A., Curry, W.B., Lutringer, A., 2003, Stable isotopes in deep-sea corals and a new mechanism for "vital effects". *Geochim. Cosmochim. Acta*,. 6, 129-1143

Affek, H. P., M. Bar-Matthews, A. Ayalon, A. Matthews, and J. M. Eiler (2008), Glacial/interglacial temperature variations in Soreq cave speleothems as recorded by 'clumped isotope' thermometry *Geochim. Cosmochim. Acta*, 72(22), 5351-5360. doi: 10.1016/j.gca.2008.06.031

Allemand D, Cuif J-P, Watabe N, Oishi M, Kawaguchi T., 1994, The organic matrix of skeletal structures of the Mediterranean Red Coral, Corallium rubrum. In: Allemand D, Cuif J-P (eds) Biomineralisation '93: 7th Int Symp Biomineralisation. *Bulletin de l'Institut oceanographique*, Monaco, Numero special 14, 1:129–140.

Allison N., Finch A., EIMF. 2000 $\delta^{11}B$, Sr, Mg and B in a modern *Porites* coral: the relationship between calcification site pH and skeletal chemistry *Geochim. Cosmochim. Acta*, 74, 1790-1800.

Beck W.C., Grossman E. L., Morse, J. W. Experimental studies of oxygen isotope fractionation in the carbonic acid system at 15, 25, and 40 C. *Geochim. Cosmochim. Acta* 69, 3493-3503.

Blamart D., Rollion-Bard C., Meibom A., Cuif J.-P., Julliet-Leclerc A., and Dauphin Y. Correlation of boron isotopic composition with ultrastructure in the deep-sea coral Lophelia pertusa: Implications for biomineralization and paleo-pH. *Geochem. Geophys. Geosys.* DOI: 10.1029/2007GC001686.

Boyer, T.P., J. I. Antonov, O. K. Baranova, C. Coleman, H. E. Garcia, A. Grodsky, D. R. Johnson, R. A. Locarnini, A. V. Mishonov, T.D. O'Brien, C.R. Paver, J.R. Reagan, D. Seidov, I. V. Smolyar, and M. M. Zweng, 2013: World Ocean Database 2013, NOAA Atlas NESDIS 72, S. Levitus, Ed., A. Mishonov, Technical Ed.; Silver Spring, MD, 209 pp.

Came, R. E., J. M. Eiler, J. Veizer, K. Azmy, U. Brand, and C. R. Weidman (2007), Coupling of surface temperatures and atmospheric CO_2 concentrations during the Palaeozoic era, *Nature*, 449(7159), 198-201. doi: 10.1038/nature06085

Came, R. E., Brand, U., Affek, H.P. (2014), Clumped isotope signatures in brachiopod carbonate. *Chem. Geol.* 377, 20-30.

Cohen A.L., McConnaughey T.A., 2003, A geochemical perspective on coral mineralization. In: Dove M, Weiner S, de Yoreo J (eds) Biomineralization. *Rev Miner Geochem* 54:151–187

Daëron, M., W. Guo, J. Eiler, D. Genty, D. Blamart, R. Boch, R. Drysdale, R. Maire, K. Wainer, and G. Zanchetta (2011), $^{13}C^{18}O$ clumping in speleothems: Observations from natural caves and precipitation experiments, *Geochim. Cosmochim. Acta,* 75(12), 3303-3317. doi: 10.1016/j.gca.2010.10.032.

Defliese, W. F., Hren, M. T., & Lohmann, K. C. (2015). Compositional and temperature effects of phosphoric acid fractionation on Δ_{47} analysis and implications for discrepant calibrations. *Chem. Geol*., 396, 51-60.

Defliese, W. F., & Lohmann, K. C. (2015). Non-linear mixing effects on mass-47 CO_2 clumped isotope thermometry: Patterns and implications. *Rapid. Comm. in Mass Spec*., 29(9), 901-909.

Dennis, K. J., and Schrag, D. P. (2010), Clumped isotope thermometry of carbonatites as an indicator of diagenetic alteration: *Geochim. Cosmochim. Acta*, v. 74, no. 14, p. 4110–4122.

Dennis, K. J., H. P. Affek, B. H. Passey, D. P. Schrag, and J. M. Eiler (2011), Defining an absolute reference frame for 'clumped' isotope studies of CO_2, *Geochim. Cosmochim. Acta* 75, 7117-7131.

Douglas P. M. J., Affek H. P., Ivany L. C., Houben A., Sijp W., Sluijs A., Schouten S, and Pagani M. Pronounced zonal heterogeneity in Eocene southern high-latitude sea surface temperatures. *Proc. Natl. Acad. Sci. USA*. 111, 6582–6587.

Dunbar R. and Wellington G. 1981, Stable isotopes in a branching coral monitor seasonal temperature variation, *Nature* vol. 293.

Eagle R., Schauble E., Tripati A., Tutken T, Hulbert R, Eiler J. 2010. Body temperatures of modern and extinct vertebrates from 13C-18O bond abundances in bioapatite. 107, 10377-10382.

Eagle, R., Eiler, J., Tripati, A., Ries, J., Freitas, P., Hiebenthal, C., Wanamaker Jr., A., Taviani, M., Elliot, M., Richardson, C., Marenssi, S., Nakamura, K., Ramirez, P., Roy, K. (2013), The influence of temperature and seawater carbonate saturation state on ^{13}C-^{18}O bond ordering in bivalve mollusks, *Biogeosciences*. doi:10.5194/bgd-10-157-2013.

Eiler, J. M. (2007), "Clumped-isotope" geochemistry – The study of naturally-occurring, multiply-substituted isotopologues, *Earth Planet. Sci. Lett.*, 262, 309-327. doi: 10.1016/j.epsl.2007.08.020

Emiliani, C., Hudson, J.H., Shinn, E.A., and George, R.Y., 1978, Oxygen and Carbon Isotopic Growth Record in a Reef Coral from the Florida Keys and a Deep-sea Coral from Blake Plateau: *Science*, v. 202, p. 627-629.

Epstein, S., Buchsbaum, R., Lowenstam, H.A., and Urey, H.C., 1953, Revised Carbonate-Water Isotopic Temperature Scale: *Geol. Soc. of Am. Bull.,* v. 64, p. 1315-1325.

Gabitov R. I., Watson E. B., Sadekov A. Oxygen isotope fractionation between calcite and fluid as a function of growth rate and temperature: An in situ study. *Chem Geol.* 4, 92-102.

Gaetani, G.A., Cohen, A.L., Wang, Z., and Crusius, J., 2011, Rayleigh-based, multi-element coral thermometry: A biomineralization approach to developing climate proxies: Geochimica Et Cosmochimica Acta, v. 75, p. 1920-1932.

Ghosh, P., J. Adkins, H. Affek, B. Balta, W. Guo, E. A. Schauble, D. Schrag, and J. M. Eiler 2006, ^{13}C-^{18}O bonds in carbonate materials: A new kind of paleothermometer, *Geochim. Cosmochim. Acta*, 70, 1439-1456. doi: 10.1016/j.gca.2005.11.014

Ghosh P., Eiler J, Campana S, Feeney R. 2007. Calibration of the carbonate 'clumped isotope' paleothermometer for otoliths. *Geochim. Cosmochim. Acta*, 71, 2736-2744.

Guo, W., J. L. Mosenfelder, W. A. Goddard III, and J. M. Eiler (2009), Isotopic fractionations associated with phosphoric acid digestion of carbonate minerals: Insights from first-principles theoretical modeling and clumped isotope measurements, *Geochim. Cosmochim. Acta*, 73(24), 7203-7225. doi: 10.1016/j.gca.2009.05.071

Grossman, E.L., and Ku, T.-L., 1986, Carbon and oxygen isotopic fractionation in biogenic aragonite- temp effects: Chemical Geology v. 59, p. 74.

Henkes G.A., Passey B.H., Wanamaker A.D., Grossman E.L., Ambrose W.G., and Carroll M.L. (2013), Carbonate clumped isotope compositions of modern marine mollusk and brachiopod shells, *Geochim. Cosmochim. Acta*, 106, 307-325. doi: 10.1016/j.gca.2012.12.020.

Henkes, G. A., Passey, B. H., Grossman, E. L., Shenton, B. J., Pérez-Huerta, A., & Yancey, T. E. (2014). Temperature limits for preservation of primary calcite clumped isotope paleotemperatures. *Geochim. Cosmochim. Acta*,139, 362-382.

Hill, P. S., Tripati, A. K., & Schauble, E. A., 2014, Theoretical constraints on the effects of pH, salinity, and temperature on clumped isotope signatures of dissolved inorganic carbon species and precipitating carbonate minerals. *Geochim. Cosmochim. Acta*, 125, 610-652.

Hill, T.M., Spero, H. J., Guilderson, T., Lavigne, M., Clague, D., Macalello, S., and Jang, N. 2011. Temperature and vital effect controls on bamboo coral (Isididae) isotope geochemistry: A test of the "lines method". *Geochem. Geophys. Geosys*., v. 12, n. 4.

Huntington, K. W., J. M. Eiler, H. P. Affek, W. Guo, M. Bonifacie, L. Y. Yeung, N. Thiagarajan, B. Passey, A. Tripati, M. Daëron, and R. Came (2009), Methods and limitations of 'clumped' CO_2 isotope (Δ_{47}) analysis by gas-source isotope ratio mass spectrometry, *J. Mass. Spectrom.*, 44(9), 1318-1329. doi: 10.1002/jms.1614

Karl, D.M. and Lukas, 1996, The Hawaii Ocean Time-series (HOT) Program: Background, rationale and field implementation. *Deep Sea Res. Part II*, 43, 129-156.

Kim, S.-T., O'Neil, J. R., Hillaire-Marcel, C., and Mucci, A., 2007. Oxygen isotope fractionation between synthetic aragonite and water: Influence of temperature and Mg2+ concentration. *Geochim. Cosmochim. Acta.,* 71, 4704-4715.

Kim, S. T. and O'Neil, J. R., 1997. Equilibrium and nonequilibrium oxygen isotope effects in synthetic carbonates. *Geochim. Cosmochim. Acta.,* 61, 3461-3475.

Kimball, J. B., Dunbar R. B., and Guilderson T. P. 2014. Oxygen and carbon isotope fractionation in calcitic deep-sea corals: Implications for paleotemperature reconstructions. *Chem. Geol. 381, 223-233.*

Kluge, T., John, C. M., Jourdan, A. L., Davis, S., & Crawshaw, J. (2015). Laboratory calibration of the calcium carbonate clumped isotope thermometer in the 25–250° C temperature range. *Geochim. Cosmochim. Acta*, 157, 213-227.

Lutringer, A., Blamart, D., Frank, N., Labeyrie L. 2005. Paleotemperatures from deep sea corals: scale effects. Cold Water Corals and Ecosystems. pp 1081-1096. ed. Freiwald A., and Murray Roberts J. Springer.

McConnaughey, T., 1989a, C-13 and O-18 Isotopic Disequilibrium in Biological Carbonates.I. Patterns: *Geochim. Cosmochim. Acta*, v. 53, p. 151-162.

McConnaughey, T., 1989b, C-13 and O-18 Isotopic Disequilibrium in Biological Carbonates.II. In vitro simulation of kinetic isotope effects: *Geochim. Cosmochim. Acta*, v. 53, p. 163-161.

McConnaughey, T., 2003. Sub-equilibrium oxygen-18 and carbon-13 levels in biological carbonates: carbonate and kinetic models. *Coral Reefs* v 22, p. 316-327.

McCrea, J.M. 1950, On the Isotopic Chemistry of Carbonates and a Paleotemperature Scale. *J. Chem. Phys.* v 18, p. 849.

Nielson L. C., DePaulo D. J., De Yoreo J. J. Self-consistent ion-by-ion growth model for kinetic isotopic fractionation during calcite precipitation. *Geochim. Cosmochim. Acta.* 86, 166-171.

Noé , S.U., and Dullo, W.C., 2006, Skeletal morphogenesis and growth mode of modern and fossil deep-water isidid gorgonians (Octocorallia) in the West Pacific (New Zealand and Sea of Okhotsk): Coral Reefs, v. 25, p. 303-320.

Passey, B. H., & Henkes, G. A. (2012). Carbonate clumped isotope bond reordering and geospeedometry. Earth and Planetary Science Letters, 351, 223-236.

Passey, B. H., N. E. Levin, T. E. Cerling, F. H. Brown, and J. M. Eiler (2010), High-temperature environments of human evolution in East Africa based on bond ordering in paleosol carbonates, *Proc. Natl. Acad. Sci. USA*, 107(25), 11245-11249. doi: 10.1073/pnas.1001824107.

Petrizzo D., Young E., Runnegar B. 2014. Implications for high-precision measurement of ^{13}C-^{18}O bonds in CO_2 and effects on carbonate clumped-isotope thermometry in modern bivalved mollusc shells. *Geochim. Cosmochim. Acta.* 142, 400-410.

Petryshyn, V., Lim, D., Brady, A., Slater, G., Laval, B., and Tripati A., 2015, Reconstruction of hydrology from microbialites using carbonate clumped isotope paleothermometer, *Geobiology,* 13, 53-67.

Robinson, L.F., Adkins, J.F., Scheirer, D.S., Fernandez, D.P., Gagnon,A., Waller,R.G., 2007. Deep-seascleractinian coral age and depth distributions in the WN Atlantic for the last 225 thousand years: *Bull.Mar.Sci.* 81,371–391.

Rollion-Bard C., Chaussidon M. and France-Lanord C. 2003 pH control on oxygen isotopic composition of symbiotic corals. *Earth Planet. Sci. Lett.* 215, 275–288.

Rollion-Bard C., Blamart D., Cuif J-P., Dauphin Y. 2010. *In situ* measurements of oxygen isotopic composition in deep-sea coral, *Lophelia pertusa*: Re-examination of the current geochemical models of biomineralization. *Geochim. Cosmochim. Acta*, 74, 1338-1349.

Rollion-Bard C., Blamart D., Trebosc J., Tricot G., Mussi A., Cuif J-P. 2011. Boron isotopes as pH proxy: A new look at boron speciation in deep-sea corals using ^{11}B MAS NMR and EELS. *Geochim. Cosmochim. Acta* 75, 1003-1012.

Saenger, C., H.P. Affek, T. Felis, N. Thiagarajan, J.M. Lough, and M. Holcomb (2012), Carbonate clumped isotope variability in shallow water corals: Temperature dependence and growth-related vital effects. *Geochim. Cosmochim. Acta*, 99, 224-242. doi: 10.1016/j.gca.2012.09.035.

Saenger, C., Affek H. P., Felis T., Thiagarajan N., Lough J. M., Holcomb M. 2013 Carbonate clumped isotope variability in shallow water corals: Temperature dependence and growth-related vital effects. *Geochim. Cosmochim. Acta*. 99, 224-242.

Schauble, E. A., P. Ghosh, and J. M. Eiler (2006), Preferential formation of 13C–18O bonds in carbonate minerals, estimated using first-principles lattice dynamics *Geochim. Cosmochim. Acta*, 70(10), 2510-2529. doi: 10.1016/j.gca.2006.02.011.

Smith, J.E., Schwarcz, H.P., Risk, M.J., McConnaughey, T.A., and Keller, N., 2000, Paleotemperatures from deep-sea corals: Overcoming 'vital effects': *Palaios*, v. 15, p. 25-32.

Swart P. K., Burns S., Leder S. 1991. Fractionation of the stable isotopes of oxygen and carbon in carbon dioxide during the reaction of calcite with phosphoric acid as a function of temperature and technique. *Chem. Geol.* 86, 89-96.

Tang, J., Dietzel, M., Fernandez, A., Tripati, A. K., & Rosenheim, B. E. (2014). Evaluation of kinetic effects on clumped isotope fractionation (Δ 47) during inorganic calcite precipitation. *Geochim. Cosmochim. Acta*,, 134, 120-136.

Tarutani, T., Clayton, R.N., and Mayeda, T.K., 1969, Effect of Polymorphism and Magnesium Substitution on Oxygen Isotope Fractionation between Calcium Carbonate and Water: *Geochim. Cosmochim. Acta*, v. 33, p. 987.

Thiagarajan, N., Adkins, J., and Eiler, J., 2011, Carbonate clumped isotope thermometry of deep-sea corals and implications for vital effects: *Geochim. Cosmochim. Acta*,, v. 75, p. 4416-4425.

Thiagarajan, N., Gerlach D., Roberts M., Burke A, McNichol A., Jenkins W., Subhas A., Thresher R., Adkins J. 2013. Movement of deep-sea coral populations on climatic timescales. 28, 227-236.

Tripati, A. K., R. A. Eagle, N. Thiagarajan, A. C. Gagnon, H. Bauch, P. R. Halloran, and J. M. Eiler (2010), Apparent equilibrium ^{13}C-^{18}O isotope signatures and 'clumped isotope' thermometry in foraminifera and coccoliths, *Geochim. Cosmochim. Acta*, 74(20), 5697-5717. doi: 10.1016/j.gca.2010.07.006.

Tripati, A. K., Hill, P. S., Eagle, R. A., Mosenfelder, J. L., Tang, J., Schauble, E. A., Eiler, J., Ries, J., & Henry, D., 2015. Beyond temperature: Clumped isotope signatures in dissolved inorganic carbon species and the influence of solution chemistry on carbonate mineral composition. *Geochim. Cosmochim. Acta*,, 166, 344-371.

Usdowski E., Michaelis J., Bottcher M. E. and Hoefs J. (1991) Factors for the oxygen isotope equilibrium fractionation between aqueous and gaseous CO_2, carbonic acid, bicarbonate, carbonate, and water (19°C). *Z. Phys. Chem.* 170, 237–249.

Wacker, U., Fiebig, J., and Schöne, B.R. (2013), Clumped isotope analysis of carbonates: comparison of two different acid digestion techniques, *Rapid Commun. Mass Spectrom.*, 27, 1631-1642. doi:10.1002/rcm.6609.

Wang, D., Wallace, A., Yoreo, J., Dove, P., 2009. Carboxylated molecules regulate magnesium content of amorphous calcium carbonates during calcification. Proceedings of the National Academy of Sciences 106, 21511–21516.

Watkins J. M., Nielson L. C., Ryerson F., DePaolo D., The influence of kinetics on the oxygen isotope composition of calcium carbonate. *Earth Planet. Sci Lett.* 375, 349-360.

Watson, E. B. 2004. A conceptual model for near-surface kinetic controls on the trace-element and stable-isotope composition of abiogenic calcite. *Geochim. Cosmochim. Acta*, 68, 1473-1488.

Watson, E. B. and Liang Y. 1995. A simple model for sector zoning in slowly-grown crystals: Implications for growth rate and lattice diffusion, with emphasis on accessory minerals in crustal rocks. *Am. mineral.* 80, 1170-1187.

Weber J., and Woodhead, P. 1972. Temperature dependence of oxygen-18 concentration in reef coral carbonates. *J. Geophys. Res.* 77, 463-473.

Zaarur, S., G. Olack, and H.P. Affek 2011, Paleo-environmental implications of clumped isotopes in land snail shells, *Geochim. Cosmochim. Acta*, 75(22), 6859-6869. doi: 10.1016/j.gca.2011.08.044.

Zaarur, S., Affek, H.P., and Brandon, M.T. 2013, A revised calibration of the clumped isotope thermometer, *Earth Planet. Sci. Lett,* v382, 47-57. doi: 10.1016/j.epsl.2013.07.026

Zeebe, R. E., 1999. An explanation of the effect of seawater carbonate concentration on foraminiferal oxygen isotopes. *Geochim. Cosmochim. Acta,* 63, 2001-2007.

Zeebe, R. E. and Wolf-Gladrow. CO_2 in Seawater: Equilibrium, Kinetics, Isotopes. Elsevier Oceanography Series, 65, pp. 346, Amsterdam, 2001

Zeebe R. E. 2007 An expression for the overall oxygen isotope fractionation between the sum of dissolved inorganic carbon and water. *Geochem. Geophys. Geosyst.* 8, Q09002.

Table captions

Table 1. Thirteen scleractinian and gorgonian deep-sea corals were collected live by submersible diving with depth and temperature measured at the time of collection. Temperature ranges are mean with standard deviation and come from Hawaii Ocean Time Series (Karl and Lukas, 1996) and cruises extracted from the National Ocean Database (Boyer et al., 2013).

Table 2. Coral specimens analyzed for $\delta^{13}C$, $\delta^{18}O$ and Δ_{47}. Δ_{47} is reported relative to the absolute reference frame (ARF). Standard error, 1σ, is reported with number of replicate measurements (n). Individual analyses are reported in Supplementary Table 1. Values are calculated using a 25 to 90 ^{o}C AFF = 0.092 (denoted by 1; Henkes et al., 2013) and AFF = 0.082 (denoted by 2; Defliese et al., 2015 and Passey et al., 2010).

Table 3. Average standard values with standard error reported for the two periods of time when samples were measured compared to accepted values. Δ_{47} values are in ‰ relative to the absolute reference frame. a. winter b. summer 2013. Values are calculated using a 25 to 90 ^{o}C AFF = 0.092 (denoted by 1; Henkes et al., 2013) and AFF = 0.082 (denoted by 2; Defliese et al., 2015 and Passey et al., 2010).

Table 4. Coral specimens analyzed for $\delta^{13}C$, $\delta^{18}O$ and Δ_{47}. Average Δ_{47} for all replicate measurements is reported relative to the absolute (ARF) reference frame. δ_{47} is reported relative to intra-laboratory working gas (WG). a) $\delta^{18}O_{water}$ values are from WOCE and HOTS. b) $\delta^{18}O$ predicted values are calculated using the equations reported in Kim and O'Neil (1997) for calcite and Kim et al. (2007) for aragonite. c) δ_{47} is relative to intralaboratory working gas with a known isotopic composition. d) Δ_{47} predicted value is calculated from the inorganic calibration of Ghosh et al. (2006); similar values are predicted from other inorganic calibrations including Zaarur et al. (2013) and Tripati et al. (2015).

Table 5. Two coral specimens were analyzed using different portions of their skeletons. PIV 146-6 was sampled by micromilling the outer portion of a disk (outer) as well as grinding an entire disk (whole). PV 703-3 was micromilled in both cases, but was milled in both the center and outer portion of a disk. All data and averages are reported as well as standard error, 1σ.

Figure captions

Figure 1. Sampling locations of three expeditions from which coral specimens were collected by deep-sea submersible diving. Locations approximate Warwick Seamount, Gulf of Alaska (DSRV Alvin, 2004), Hawaiian and Northwest Hawaiian Islands (DSRV Pisces V, 2005 and 2007) and Line Islands (DSRV Pisces IV, 2006).

Figure 2. a) A bamboo coral from Warwick Seamount, ALV 3808-4. The bottommost internode is cut and the disk used for milling along the outer, most recently accreted portion. b) A portion of a radial disk from PV 703-5 in which samples were milled from the center and outer portion.

Figure 3. Scleractinian and gorgonian deep-sea coral compared to deep-sea corals reported in Thiagarajan et al. (2011) and average Δ_{47} values recalculated relative to ARF from Eagle et al. (2013). Sample 703-7 is not included in the calibration is not considered live-collected.

Figure 4. Scleractinian corals from this study and Thiagarajan et al. (2011) are combined (slope: 0.0582±0.008, intercept: 0.0452±0.103, R^2=0.81) and along with gorgonian deep-sea corals are compared to other reported calibrations studies.

Figure 5. Scleractinian and gorgonian corals from this study and Thiagarajan et al. (2011) are compared to the theoretical predictions for Δ_{63} for aragonite, calcite and dolomite. Acid fractionation values were added to convert to Δ_{47}.

Figure 6. Sensitivity analysis of varying acid digestion fractionation factor ($\Delta_{25\text{-}90}$) on results.

Figure 7. Δ_{47} residuals are calculated from average measured Δ_{47} values for each coral relative to the inorganic calibrations of Ghosh et al. (2006), Zaruur et al. (2013) and Dennis and Schrag (2010). $\delta^{18}O$ residuals are calculated from average measured $\delta^{18}O$ values relative to the calibrations of Kim and O'Neil (1997) and Kim et al. (2007) for calcite and aragonite, respectively.

Figure 8. Δ_{47} residuals are calculated from average measured Δ_{47} values for each coral relative to the biogenic calibrations of Eagle et al. (2013). $\delta^{18}O$ residuals are calculated from average measured $\delta^{18}O$ values relative to the calibrations of Kim and O'Neil (1997) and Kim et al. (2007) for calcite and aragonite, respectively.

Figure 9. Δ_{47} residuals are calculated from average measured Δ_{47} values for each coral relative to the theoretical calibration of Schauble et al. (2006) paired with theoretical acid digestion

fractionations from Guo et al. (2009). $\delta^{18}O$ residuals are calculated from average measured $\delta^{18}O$ values relative to the calibrations of Kim and O'Neil (1997) and Kim et al. (2007) for calcite and aragonite, respectively.

Figure 10. Schematic illustrating general trajectories for different processes on stable isotope signatures (Δ_{63} or Δ_{47} values and $\delta^{18}O$), relative to an arbitrary point. Equilibrium temperature dependence is shown (Ghosh et al., 2006). Note that mixing of DIC from different sources results in curved trajectories (in $\delta^{18}O$ space, mixing is linear whereas in Δ_{47} space can be non-linear) (Eiler and Schauble, 2004; Thiagarajan et al., 2011; Defliese and Lohmann, 2015). Diffusion results in enrichment of clumped species and depletion in $\delta^{18}O$ (Thiagarajan et al., 2011). CO_2 hydration reactions are strongly temperature pH-dependent and also result in enrichment of clumped species and depletion in $\delta^{18}O$ (Affek, 2013; Tang et al., 2014; Tripati et al., 2015). At any given temperature, equilbrium DIC species have differing clumped and oxygen isotope signatures, potentially also giving rise to pH effect (Hill et al., 2014; Tripati et al., 2015). Solid-state diffusion processes (Passey and Henkes, 2012; Henkes et al., 2014), including hypothesized reordering in the interfacial region (Tripati et al., 2015) only influence clumped isotope signatures and not bulk isotopic signatures (e.g., $\delta^{18}O$).

Figure 11. Schematic of the scleractinian coral calcifying region (modified from McConnaughey, 1989; Adkins et al., 2003) illustrating processes that are hypothesized to result in stable isotope signatures observed in corals. Calcium pumping across the cell wall establishes a pH gradient between seawater and the extracellular calcifying fluid. Within the calcifying fluid, carbon can be sourced from CO_2 that is diffusively transported across the cell wall, and/or through seawater leakage. The hydration and/or hydroxylation of CO_2 are slow reactions, particularly at low temperature and at high pH, driving disequilibrium in $\delta^{18}O$ and in clumped isotope signatures. The enzyme carbonic anhydrase will catalyze this reaction, if present and sufficiently active. At a given temperature, both HCO_3^- and CO_3^{2-} ions have distinct clumped isotope and $\delta^{18}O$ signatures, and therefore changes in extracellular calcifying fluid pH may also affect the isotopic composition of minerals, as explored through various models including the pH, surface entrapment, and interfacial models mentioned in the text. Surface kinetic and interfacial processes and properties (e.g., surface speciation, attachment/detachment rates for isotopologues, the occurrence of defects, the nature of protein and saccharide macromolecules) also affect crystal growth and chemistry.

Figure 1

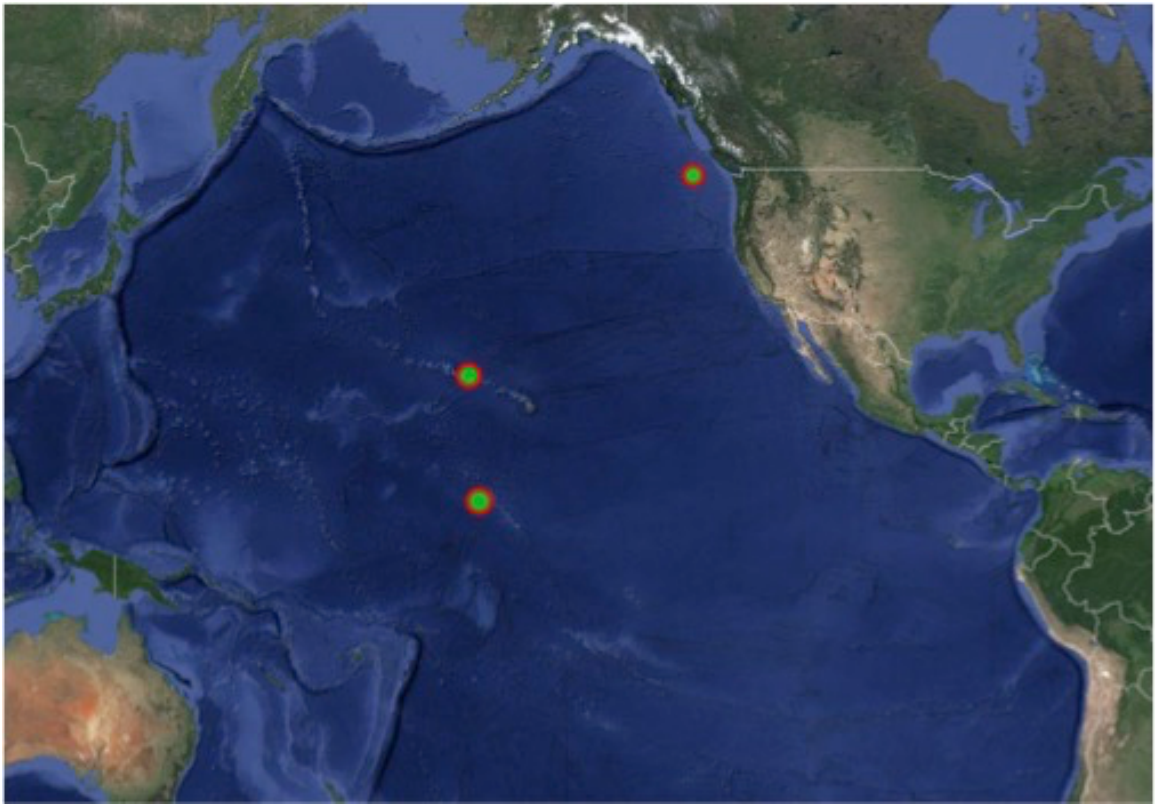

Figure 2

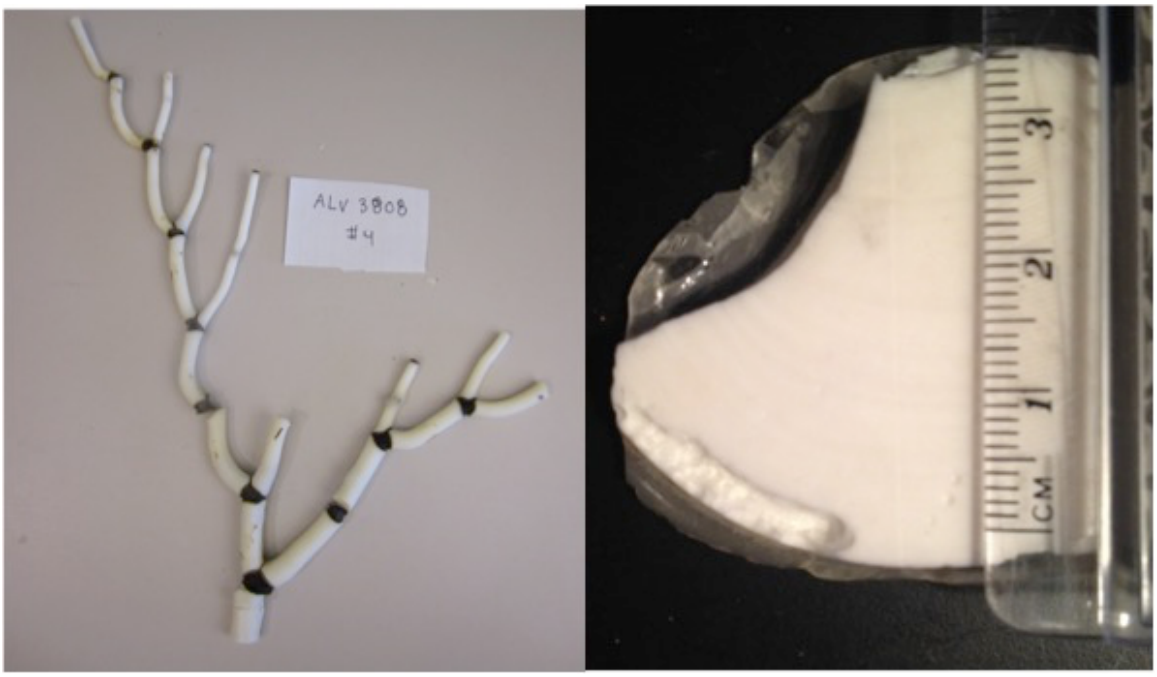

Figure 3

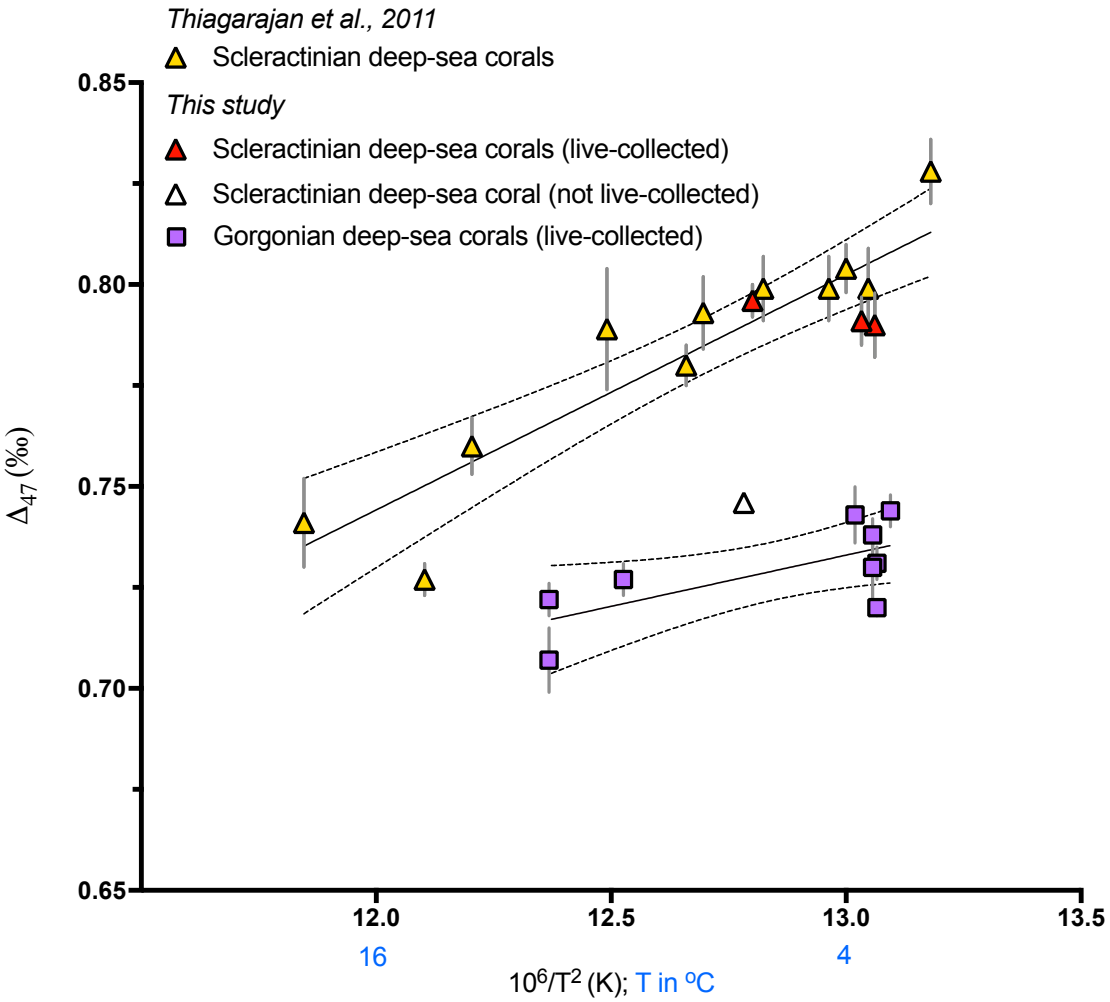
Thiagarajan et al., 2011
Scleractinian deep-sea corals
This study
Scleractinian deep-sea corals (live-collected)
Scleractinian deep-sea coral (not live-collected)
Gorgonian deep-sea corals (live-collected)
0.85
0.80
0.75
0.70
0.65
Δ47 (‰)
12.0
12.5
13.0
13.5
16
4
10^6/T^2 (K); T in °C

Figure 4

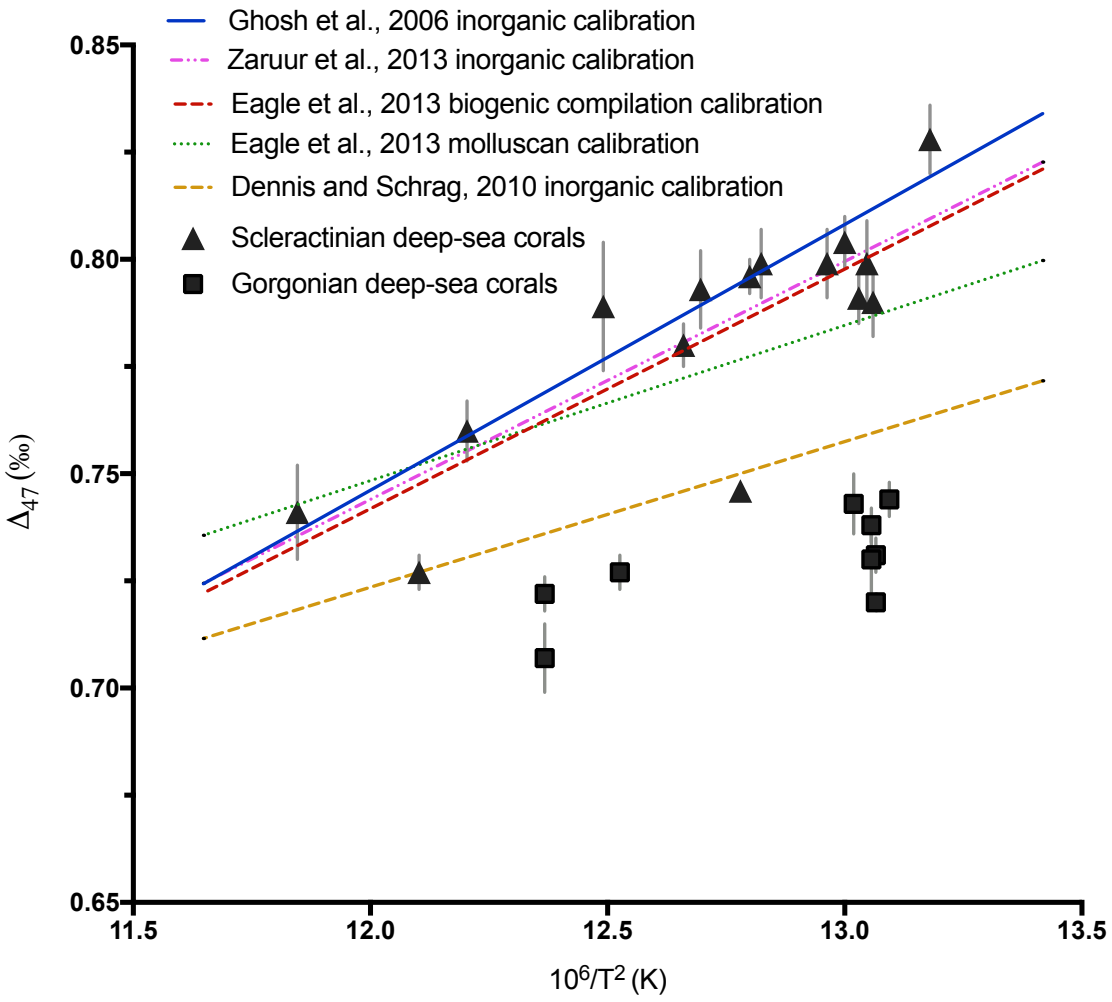
Ghosh et al., 2006 inorganic calibration
Zaruur et al., 2013 inorganic calibration
Eagle et al., 2013 biogenic compilation calibration
Eagle et al., 2013 molluscan calibration
Dennis and Schrag, 2010 inorganic calibration
Scleractinian deep-sea corals
Gorgonian deep-sea corals
0.85
0.80
0.75
0.70
0.65
11.5
12.0
12.5
13.0
13.5
Δ47 (‰)
10^6/T^2 (K)

Figure 5

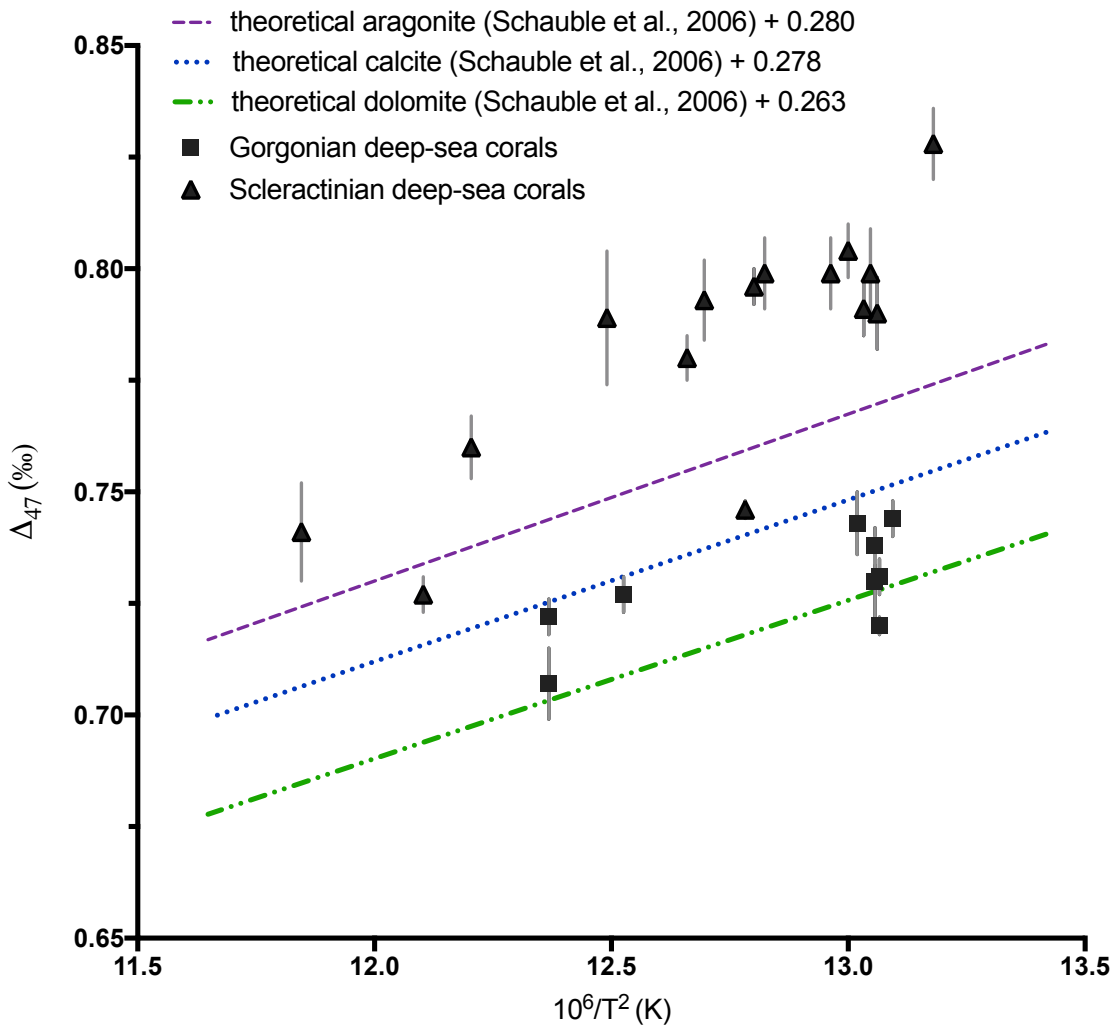
theoretical aragonite (Schauble et al., 2006) + 0.280
theoretical calcite (Schauble et al., 2006) + 0.278
theoretical dolomite (Schauble et al., 2006) + 0.263
Gorgonian deep-sea corals
Scleractinian deep-sea corals
0.85
0.80
0.75
0.70
0.65
Δ47 (‰)
11.5
12.0
12.5
13.0
13.5
10^6/T^2 (K)

Figure 6

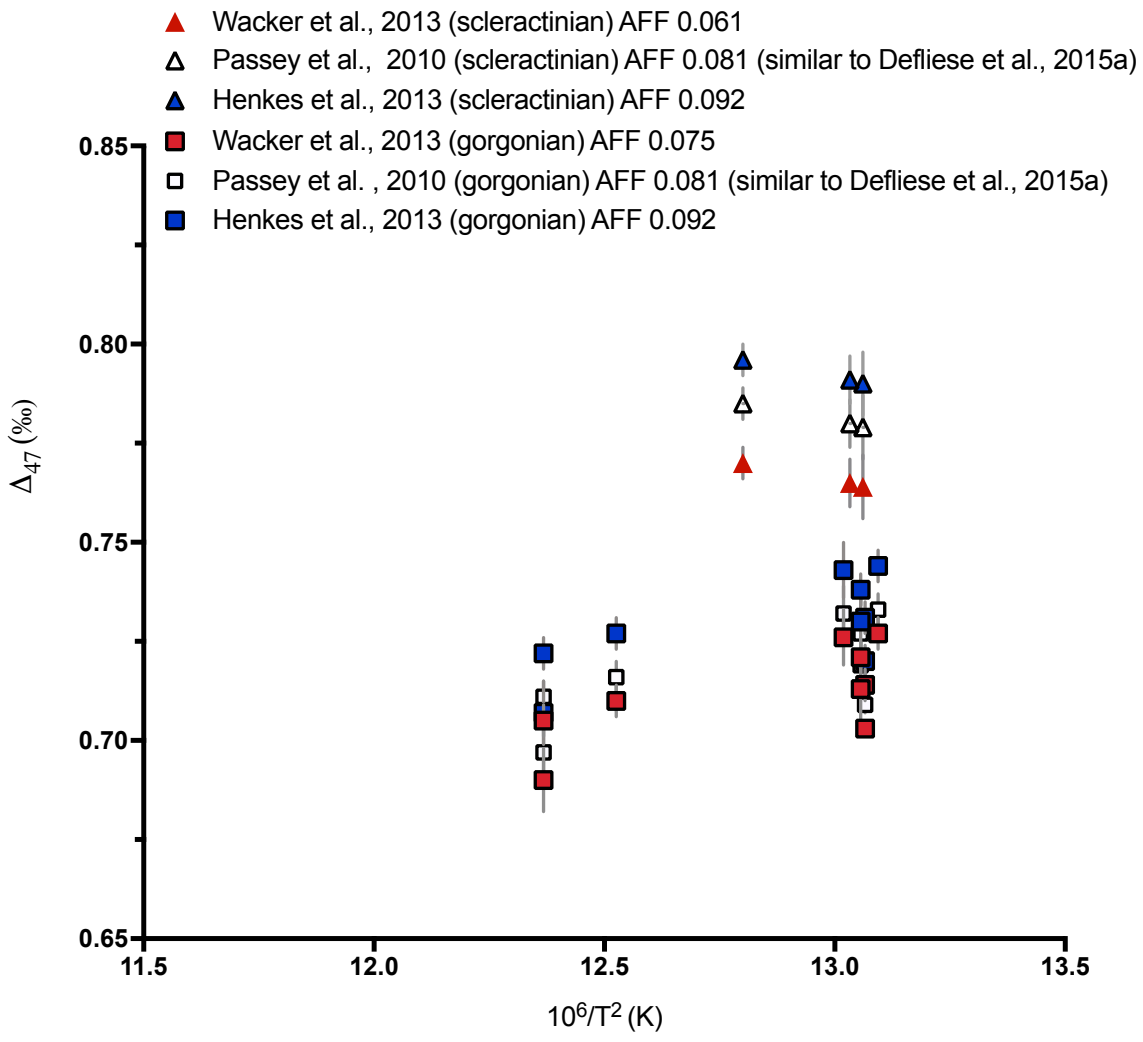
Wacker et al., 2013 (scleractinian) AFF 0.061
Passey et al., 2010 (scleractinian) AFF 0.081 (similar to Defliese et al., 2015a)
Henkes et al., 2013 (scleractinian) AFF 0.092
Wacker et al., 2013 (gorgonian) AFF 0.075
Passey et al. , 2010 (gorgonian) AFF 0.081 (similar to Defliese et al., 2015a)
Henkes et al., 2013 (gorgonian) AFF 0.092
0.85
0.80
0.75
0.70
0.65
Δ47 (‰)
11.5
12.0
12.5
13.0
13.5
10^6/T^2 (K)

Figure 7

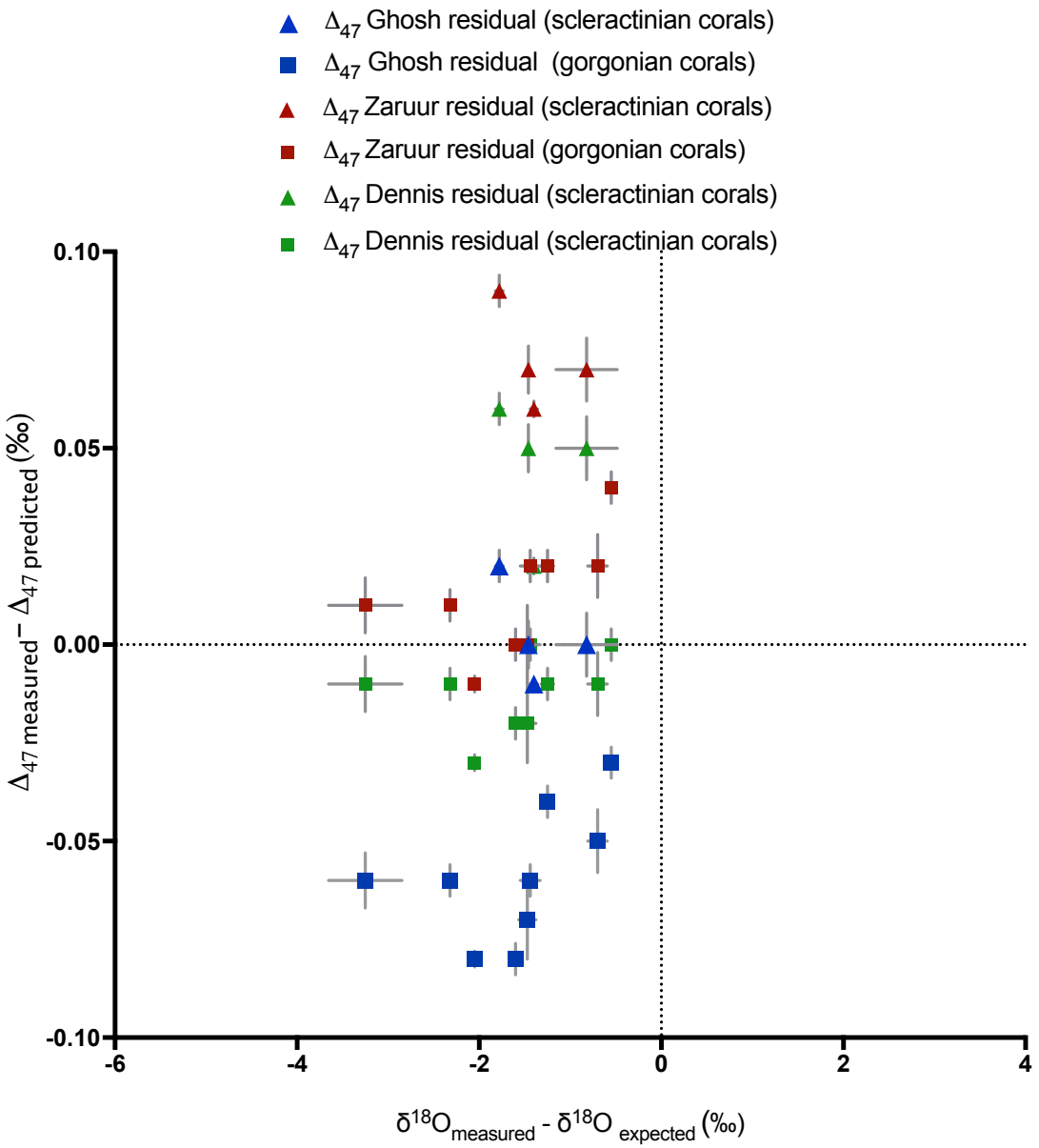
Δ47 Ghosh residual (scleractinian corals)
Δ47 Ghosh residual (gorgonian corals)
Δ47 Zaruur residual (scleractinian corals)
Δ47 Zaruur residual (gorgonian corals)
Δ47 Dennis residual (scleractinian corals)
Δ47 Dennis residual (scleractinian corals)
0.10
0.05
0.00
-0.05
-0.10
-6
-4
-2
0
2
4
Δ47 measured − Δ47 predicted (‰)
δ18Omeasured - δ18O expected (‰)

Figure 8

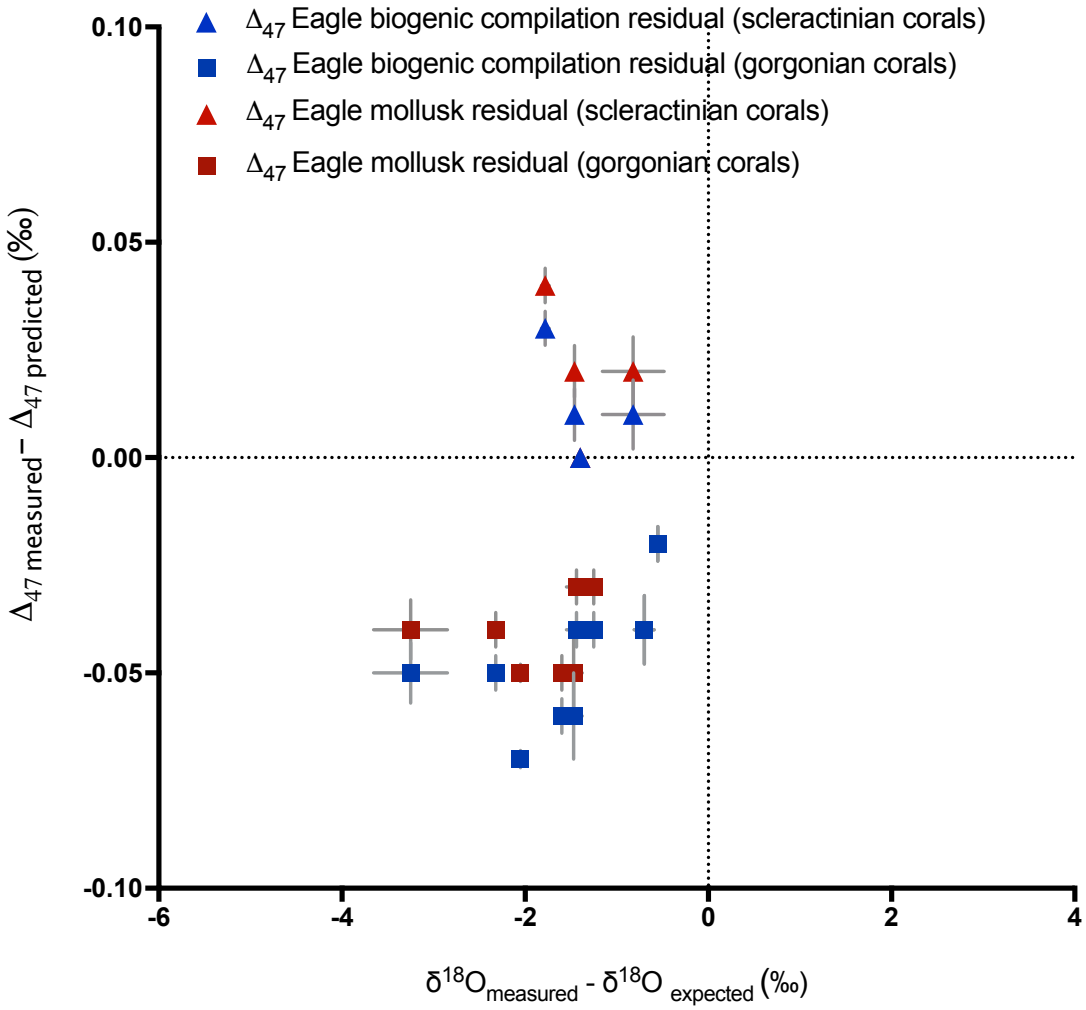
Δ47 Eagle biogenic compilation residual (scleractinian corals)
Δ47 Eagle biogenic compilation residual (gorgonian corals)
Δ47 Eagle mollusk residual (scleractinian corals)
Δ47 Eagle mollusk residual (gorgonian corals)
0.10
0.05
0.00
-0.05
-0.10
-6
-4
-2
0
2
4
Δ47 measured − Δ47 predicted (‰)
δ18Omeasured - δ18O expected (‰)

Figure 9

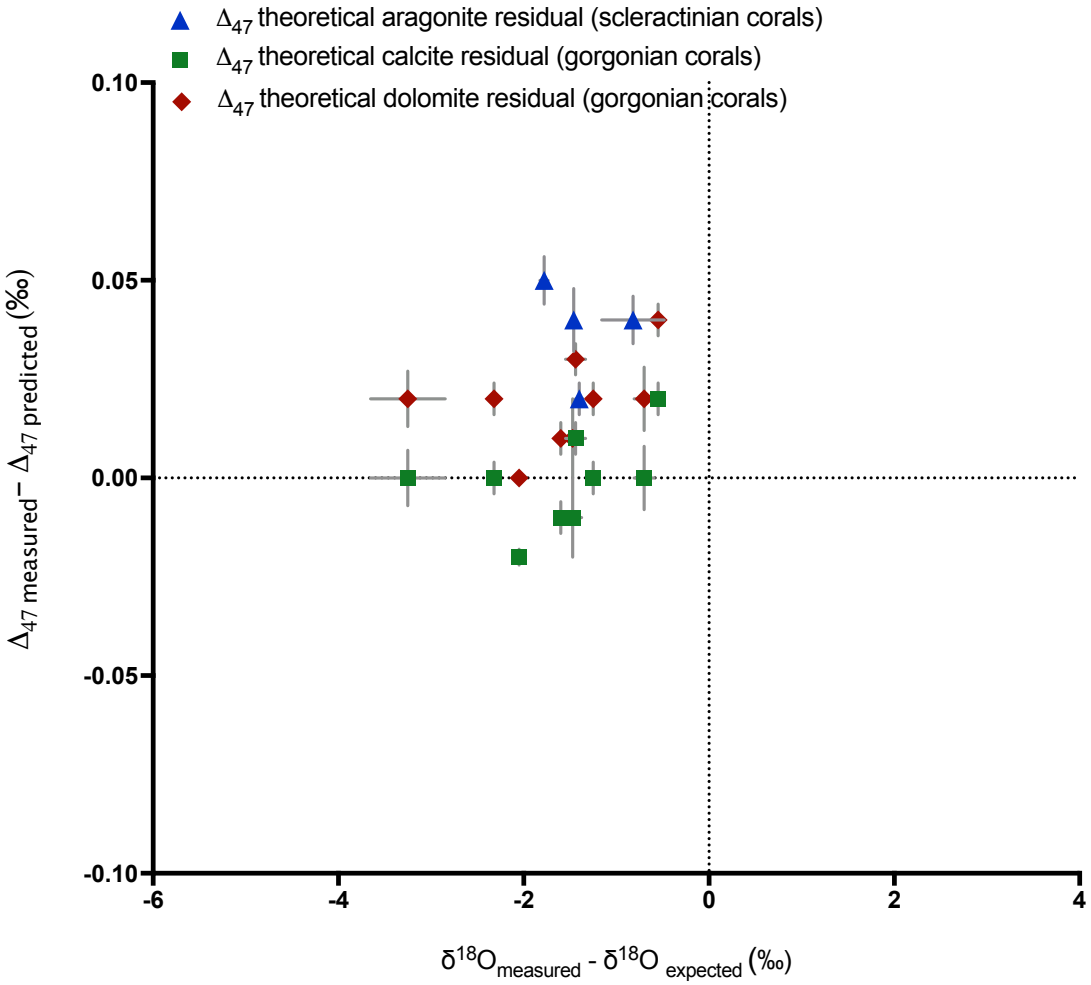
Δ47 theoretical aragonite residual (scleractinian corals)
Δ47 theoretical calcite residual (gorgonian corals)
Δ47 theoretical dolomite residual (gorgonian corals)
0.10
0.05
0.00
-0.05
-0.10
-6
-4
-2
0
2
4
Δ47 measured − Δ47 predicted (‰)
δ18Omeasured - δ18O expected (‰)

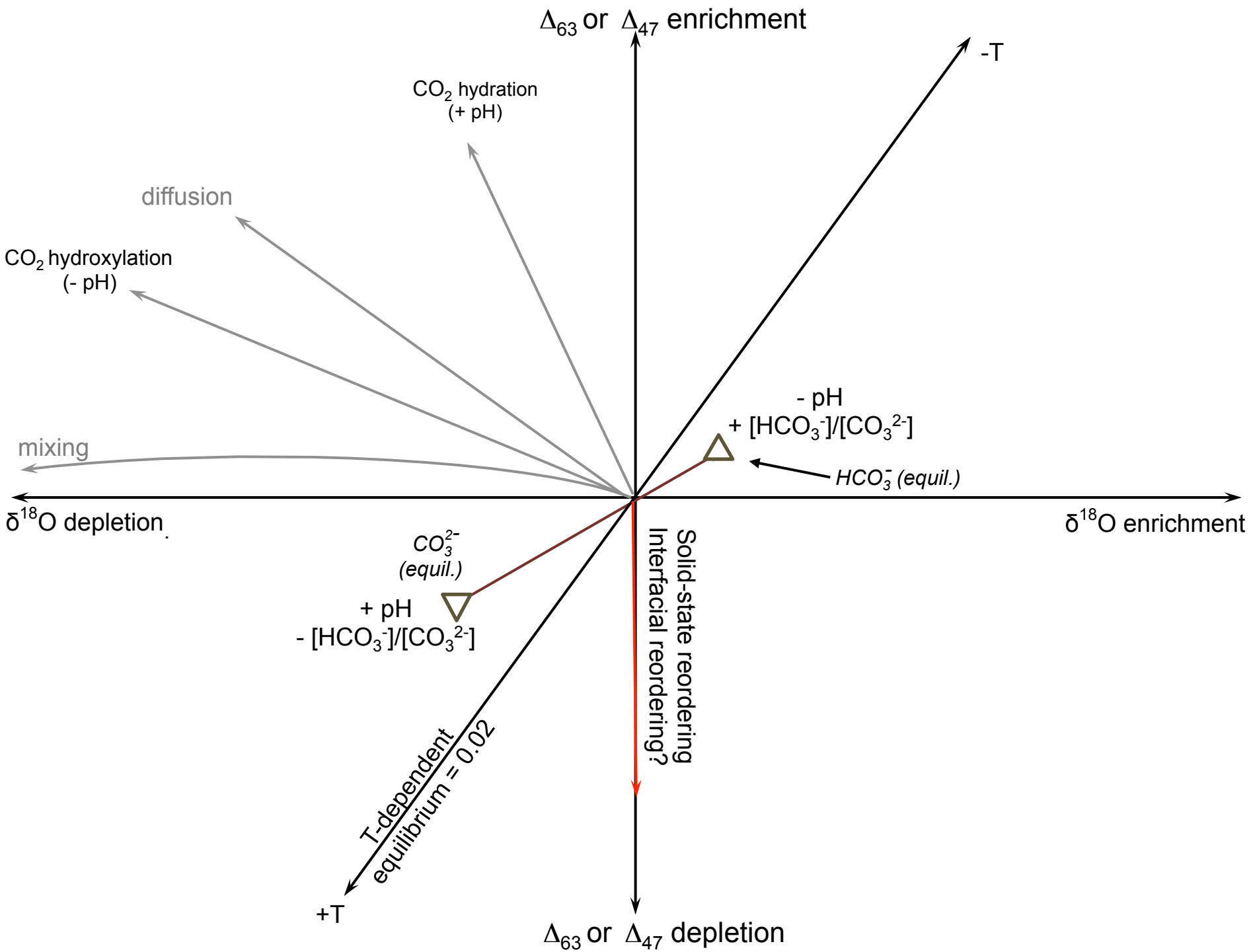
Δ_{63} or Δ_{47} enrichment
-T
CO_2 hydration
(+ pH)
diffusion
CO_2 hydroxylation
(- pH)
mixing
- pH
+ $[HCO_3^-]/[CO_3^{2-}]$
HCO_3^- (equil.)
$\delta^{18}O$ depletion
$\delta^{18}O$ enrichment
CO_3^{2-}
(equil.)
+ pH
- $[HCO_3^-]/[CO_3^{2-}]$
Solid-state reordering
Interfacial reordering?
T-dependent
equilibrium = 0.02
+T
Δ_{63} or Δ_{47} depletion

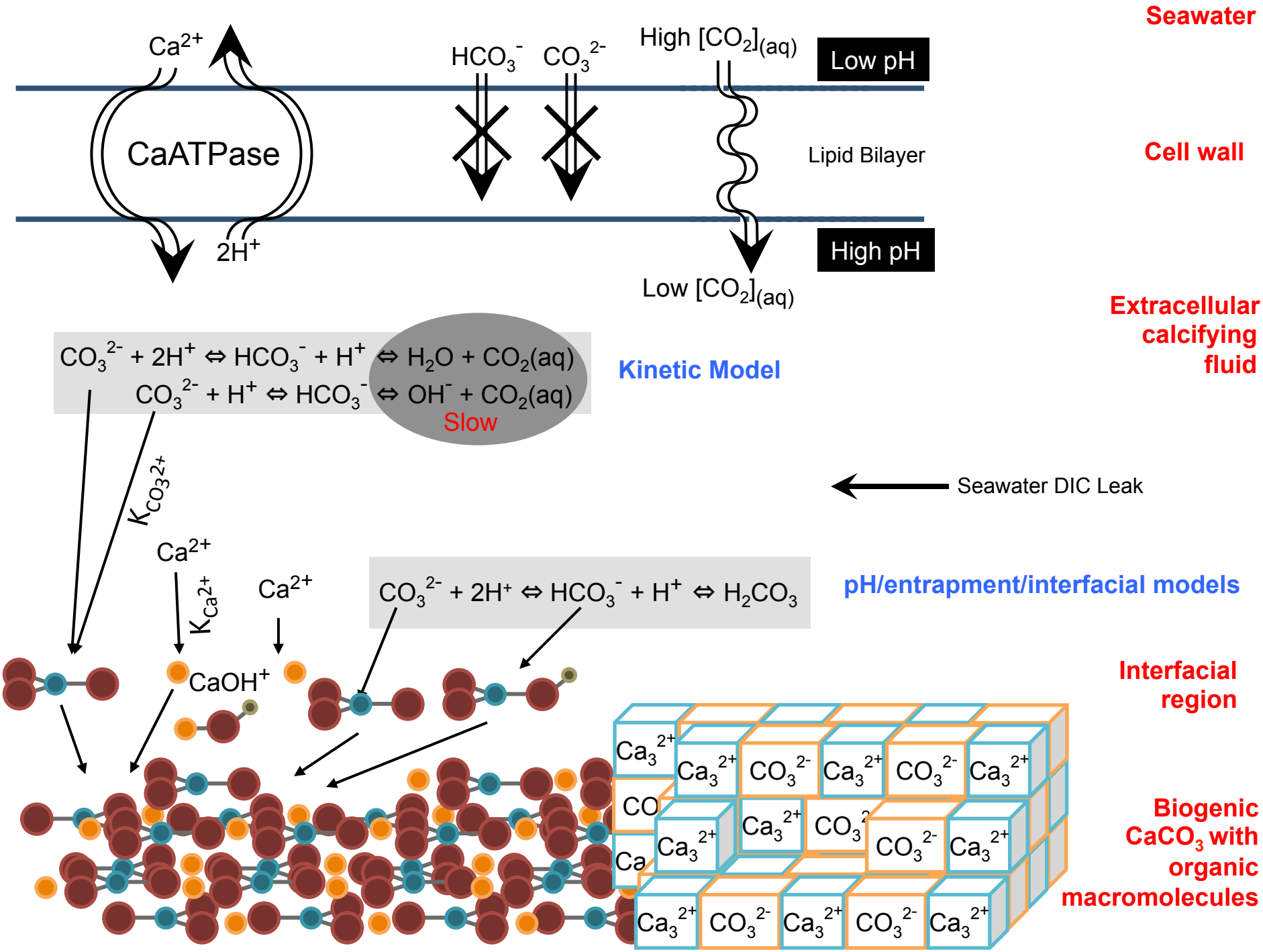
Seawater
Cell wall
Extracellular calcifying fluid
Interfacial region
Biogenic $CaCO_3$ with organic macromolecules
Ca^{2+}
CaATPase
$2H^+$
HCO_3^-
CO_3^{2-}
High $[CO_2]_{(aq)}$
Low pH
Lipid Bilayer
High pH
Low $[CO_2]_{(aq)}$
$CO_3^{2-} + 2H^+ \Leftrightarrow HCO_3^- + H^+ \Leftrightarrow H_2O + CO_2(aq)$
$CO_3^{2-} + H^+ \Leftrightarrow HCO_3^- \Leftrightarrow OH^- + CO_2(aq)$
Slow
Kinetic Model
$K_{CO_3^{2+}}$
$K_{Ca^{2+}}$
Seawater DIC Leak
$CO_3^{2-} + 2H^+ \Leftrightarrow HCO_3^- + H^+ \Leftrightarrow H_2CO_3$
pH/entrapment/interfacial models
$CaOH^+$
Ca_3^{2+}
CO_3^{2-}
CO
Ca

1 Table 1

ID	Order	Coral	Location	Latitude	Longitude	depth (m)	T (°C)	T range (°C)
ALV 3806-1	Gorgonacea	Isididae	Warwick, AK	48°04'N	132°48'W	872	3.2	3.4±0.1
ALV 3808-1	Gorgonacea	Isididae	Warwick, AK	48°04'N	132°48'W	758	3.5	3.5±0.1
ALV 3808-3	Gorgonacea	Isididae	Warwick, AK	48°04'N	132°48'W	720	3.5	3.7±0.1
ALV 3808-4	Gorgonacea	Isididae	Warwick, AK	48°04'N	132°48'W	704	3.6	3.7±0.1
ALV 3808-5	Gorgonacea	Isididae	Warwick, AK	48°04'N	132°48'W	634	3.6	3.8±0.2
PV 703- 5	Gorgonacea	Coralliidae	Twin Banks, NWHI	23°07N	163°08W	942	4	4.2±0.1
PV 592-1	Gorgonacea	Isididae	Big Island, HI	19°48 N	156°07'W	386	9.4	10.3±0.2
PV 694-13	Gorgonacea	Isididae	East French Frigate Shoals, NWHI	23°54'N	165°23'W	356	11.2	10.6±0.6
PV 694-3	Gorgonacea	Isididae	East French Frigate Shoals, NWHI	23°54'N	165°23'W	351	11.2	11.1±0.7
PV 703-2	Scleractinia	*E.rostrata*	Twin Banks, NWHI	23°07N	163°08W	1108	3.7	3.7±0.1
PIV 146-6	Scleractinia	*E.rostrata*	Kingman Reef	06° 26.0 N	162° 27.5 W	788	4	5.5±0.2
PIV 148-2	Scleractinia	*E.rostrata*	Palmyra Atoll	05° 50.784 N	162° 06.741 W	588	6.5	6.9±0.4
PV 703-7	Scleractinia	*E.rostrata*	Twin Banks, NWHI	23°07N	163°08W	534	6.7	6.7±0.3

2

3

1 Table 2

ID	Order	mineral	n	$\delta^{13}C$ (‰ VPDB)	$\delta^{18}O$ (‰ VPDB)	Δ_{47} (‰ ARF; 90°C results)	Δ_{47} (‰ ARF; adj. 25°C[1])	Δ_{47} (‰ ARF; adj. 25°C
ALV 3806-1	Gorgonacea	high-Mg calcite	8	-3.74 (±0.091)	0.76 (±0.109)	0.663 (±0.004)	0.744 (±0.004)	0.734 (±0.004)
ALV 3808-1	Gorgonacea	high-Mg calcite	3	-3.15 (±0.024)	0.53 (±0.064)	0.650 (±0.004)	0.731 (±0.004)	0.721 (±0.004)
ALV 3808-3	Gorgonacea	high-Mg calcite	2	-4.58 (±0.04)	0.08 (±0.025)	0.639 (±0.002)	0.720 (±0.002)	0.710 (±0.002)
ALV 3808-4	Gorgonacea	high-Mg calcite	6	-3.15 (±0.208)	0.66 (±0.095)	0.649 (±0.01)	0.730 (±0.01)	0.720 (±0.01)
ALV 3808-5	Gorgonacea	high-Mg calcite	3	-5.87 (±0.131)	-0.21 (±0.043)	0.657 (±0.004)	0.738 (±0.004)	0.728 (±0.004)
PV 703- 5	Gorgonacea	high-Mg calcite	6	-6.35(±0.543)	-1.09 (±0.345)	0.662 (±0.007)	0.743 (±0.007)	0.733 (±0.007)
PV 592-1	Gorgonacea	high-Mg calcite	2	-2.42 (±0.068)	-0.18 (±0.029)	0.646 (±0.004)	0.727 (±0.004)	0.717 (±0.004)
PV 694-13	Gorgonacea	high-Mg calcite	4	-0.71 (±0.019)	0.10 (±0.018)	0.641 (±0.004)	0.722 (±0.004)	0.712 (±0.004)
PV 694-3	Gorgonacea	high-Mg calcite	5	-4.19 (±0.108)	-0.05 (±0.154)	0.626 (±0.008)	0.707 (±0.008)	0.697 (±0.008)
PV 703-2	Scleractinia	aragonite	8	-1.91 (±0.19)	2.11 (±0.338)	0.709 (±0.008)	0.790 (±0.008)	0.780 (±0.008)
PIV 146-6	Scleractinia	aragonite	7	-2.90 (±0.166)	1.40 (±0.083)	0.710 (±0.006)	0.791 (±0.006)	0.781 (±0.006)
PIV 148-2	Scleractinia	aragonite	7	-3.90 (±0.351)	0.70 (±0.044)	0.715 (±0.004)	0.796 (±0.004)	0.786 (±0.004)
PV 703-7	Scleractinia	aragonite	3	-3.10 (±0.065)	0.40 (±0.038)	0.665 (±0.002)	0.746 (±0.002)	0.736 (±0.002)

2

3

1 Table 3

Standard	n	Δ_{47} UCLA (‰ ARF; adj. 25°C[1])	Δ_{47} UCLA (‰ ARF; adj. 25°C[2])	Accepted Δ_{47} (Caltech) (‰ ARF; adj. 25°C)
Cararra marble[a]	8	0.395 (±0.008)	0.385 (±0.008)	0.395
Cararra marble[b]	15	0.390 (±0.005)	0.380 (±0.005)	0.395
Carmel chalk[a]	7	0.688 (±0.004)	0.678 (±0.004)	0.697
Carmel chalk[b]	13	0.695 (±0.004)	0.685 (±0.004)	0.697
102-GC-AZ01[a]	5	0.729 (±0.004)	0.719 (±0.004)	0.713
102-GC-AZ01[b]	3	0.699 (±0.006)	0.689 (±0.006)	0.713
TV01/TV03[b]	7	0.720 (±0.007)	0.710 (±0.007)	0.713

2

3

Table 4

ID	$\delta^{18}O_{coral}$ (‰ VPDB)	$\delta^{18}O_{water}$ (‰ VPDB)[a]	$\delta^{18}O$ predicted (‰ VPDB)[b]	δ_{47} (‰ WG)[c]	Δ_{47} (‰ ARF; adj. 25°C)	Δ_{47} predicted (‰ ARF; adj. 25°C)[d]
ALV 3806-1	0.78 (±0.123)	-0.2	2.6	14.79	0.744 (±0.004)	0.833
ALV 3808-1	0.53 (±0.064)	-0.2	2.53	15.12	0.731 (±0.004)	0.831
ALV 3808-3	0.08 (±0.025)	-0.2	2.53	13.2	0.720 (±0.002)	0.831
ALV 3808-4	0.66 (±0.095)	-0.2	2.51	15.24	0.730 (±0.01)	0.831
ALV 3808-5	-0.21 (±0.043)	-0.2	2.51	11.66	0.738 (±0.004)	0.831
PV 703- 5	-1.70 (±0.165)	-0.05	2.26	10.11	0.743 (±0.007)	0.828
PV 592-1	-0.18 (±0.029)	0.1	0.87	15.1	0.727 (±0.004)	0.797
PV 694-13	0.10 (±0.018)	0.1	0.45	16.97	0.722 (±0.004)	0.786
PV 694-3	-0.05 (±0.154)	0.1	0.45	17.03	0.707 (±0.008)	0.786
PV 703-2	2.00 (±0.318)	-0.1	3.13	18	0.790 (±0.008)	0.830
PIV 146-6	1.40 (±0.083)	-0.1	3.06	16.289	0.791 (±0.006)	0.828
PIV 148-2	0.70 (±0.044)	0.1	2.28	14.62	0.796 (±0.004)	0.813
PV 703-7	0.40 (±0.038)	0.1	1.6	14.94	0.746 (±0.002)	0.796

Table 5

ID	n	$\delta^{13}C$ (‰ VPDB)	$\delta^{18}O$ (‰ VPDB)	Δ_{47} predicted (‰ ARF; adj. 25°C)[d]
PIV 146-6 (outer)	4	-2.67 (±0.161)	1.33 (±0.02)	0.796 (±0.007)
PIV 146-6 (whole)	3	-3.37 (±0.086)	1.77 (±0.042)	0.820 (±0.010)
PIV 146-6 (average)	7	-2.90 (±0.166)	1.40 (±0.083)	0.808 (±0.008)
PV 703- 5 (center)	3	-7.76 (±0.038)	-1.70 (±0.165)	0.760 (±0.010)
PV 703-5 (outer)	3	-4.95 (±0.116)	-0.47 (±0.025)	0.740 (±0.005)
PV 703-5 (average)	6	-6.35(±0.543)	-1.09 (±0.345)	0.750 (±0.007)